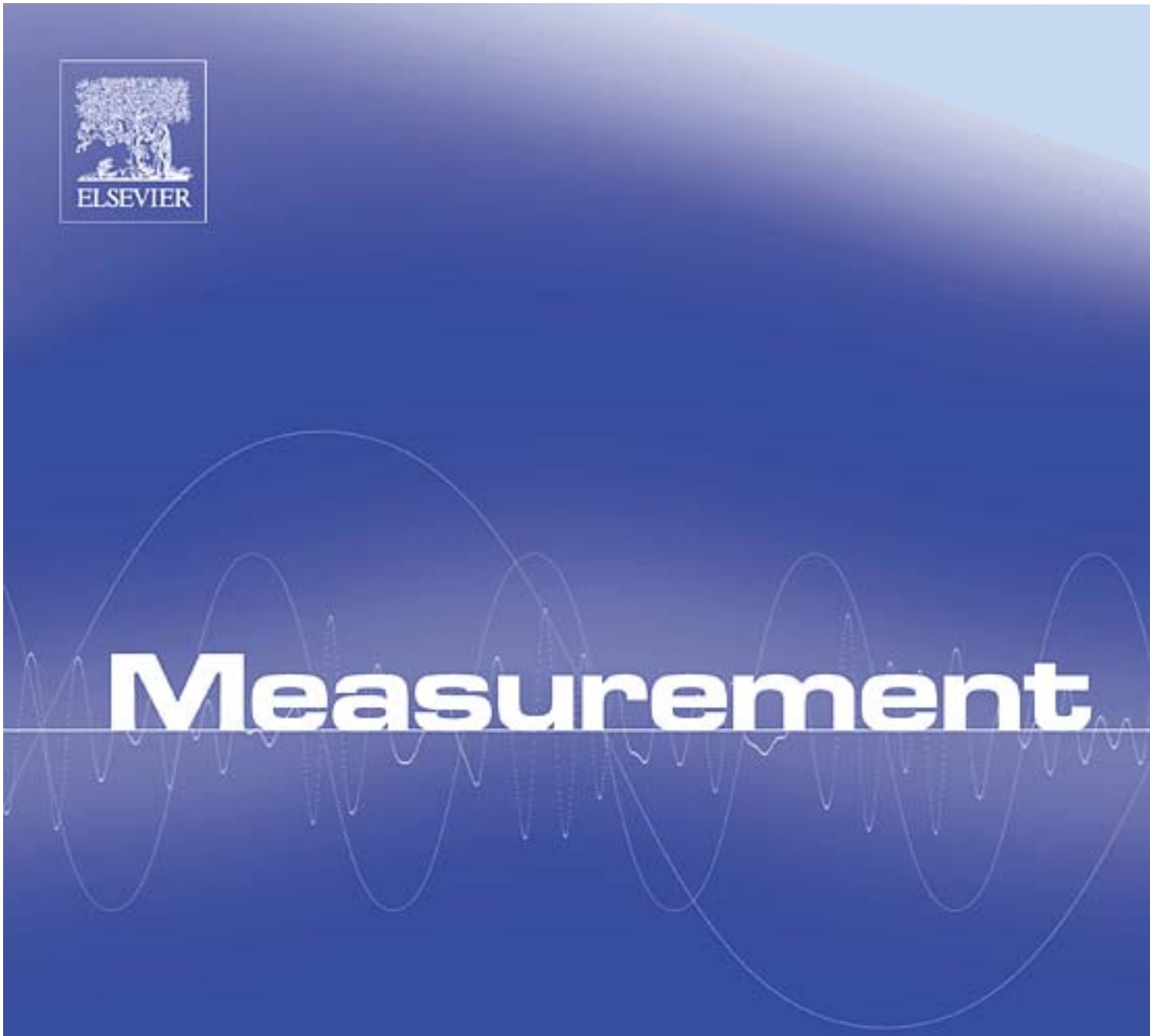

Measurement

Official Journal of the
International
Measurement
Confederation

Measurement 168 (2021) 108472

Contents lists available at ScienceDirect

Measurement

journal homepage: www.elsevier.com/locate/measurement

Experimental validation of adaptive RBFNN global fast dynamic terminal sliding mode control for twin rotor MIMO system against wind effects

Mohammed Zinelaabidine Ghellab [a], Samir Zeghlache [a,*], Ali Djerioui [b], Loutfi Benyettou [b]

[a] LASS, Laboratoire d'Analyse des Signaux et Systèmes, Department of Electrical Engineering, Faculty of Technology, University of M'sila, BP 166 Ichbilia, Msila, Algeria
[b] LGE, Laboratoire de Génie Electrique, Department of Electrical Engineering, Faculty of Technology, University of M'sila, BP 166 Ichbilia, Msila, Algeria

ARTICLE INFO

Keywords:
TRMS
RBFNN
Robust control
Wind effects
Adaptive control
Stability

ABSTRACT

In this paper, an Adaptive RBFNN global fast dynamic terminal sliding mode control (ARBFNNGFDTSMC) is designed to situate the main and tail angles of a twin rotor MIMO system (TRMS). The control objective is to stabilize the TRMS in a reference position or follow a predefined trajectory. An adaptive RBFNN has been used in order to identified unknown nonlinear dynamics of the TRMS. In addition, another adaptive control expressions has been added to diminish the wind gusts, external disturbance effects, and to compensate the estimation errors of the adaptive RBFNN. Moreover, the stability analysis in closed-loop is assured by using Lyapunov method. The developed controller is applied to the TRMS with cross coupling between tail and main subsystems without decoupling procedure. Experimental results prove the good control tracking performance in presence of wind gusts and external disturbances.

1. Introduction

As of late, advanced methods have achieved several novel ideas in aircraft conception that are different to their ancestors. The distinctions are for the most part in aircraft designs and control strategies. These flying platforms, for instance, revolving wing aircrafts and fixed-wing vehicles, among others, have obvious points of interest for surveillance and inspection missions. Nonetheless, these flying platforms are substantially more complexes with respect to the dynamics and control strategy of aircrafts, as their control inputs are torques and forces created by the main and tail rotors. Likewise, a high coupling effect between the main and tail rotors expands the system nonlinearities. These peculiarities of the system acquaint thorough difficulties with the controller synthesis and experimental implementation [1,2]. TRMS is a flexible aerodynamic system considered as test rig, its comportment is like of helicopter. Accordingly, TRMS is regularly utilized in an laboratory to test the viability of a control methodology which is intended for a genuine helicopter system. An enormous number of endeavors have been made during the previous a very long while. Many strategies are utilized to identify the dynamic model of the TRMS as presented in [3–5]. Different TRMS control strategies have been developed in literature [6–20]. Where in [6] the authors proposed a simple PID controller, In [7] a PID control has been associated with genetic algorithms in order to give an optimized control. A control strategy based on proportional integral differential active force control has been proposed in [8]. In [9] fuzzy logic techniques has been used to control the TRMS, a linear quadratic regulator (LQR) has been designed in [10], another robust control method by using nonlinear H_∞ has been synthesized in [2,11], Sliding Mode Control (SMC) strategy has been utilized in [12–15] to control TRMS. The SMC is described by robustness against uncertainties and external disturbances. Unfortunately, the chattering phenomenon incite high frequency in the control inputs. The referenced works in [16,17] proposed a solutions to decrease the chattering phenomenon in only simulation, where the authors have not provide any practical experimentation. In [18] artificial neural networks are used in order to design adaptive dynamic nonlinear model inversion control of the TRMS. In [19], the control design depend on the precise mathematical model, i.e. the TRMS model was needed to synthesis the control law. The most controls design proposed in literature address the instance of decoupling control techniques which separate main and tail subsystems as presented in [20].

In this work an adaptive control strategy has been proposed where the decoupling procedures is not required, thereby ameliorating the trajectory tracking of the TRMS. In order to further ameliorate the SMC

* Corresponding author.
E-mail addresses: mohamedzinelaabidine.ghellab@univ-msila.dz (M.Z. Ghellab), samir.zeghlache@univ-msila.dz (S. Zeghlache), ali.djerioui@univ-msila.dz (A. Djerioui), loutfi.benyettou@univ-msila.dz (L. Benyettou).

https://doi.org/10.1016/j.measurement.2020.108472
Received 2 July 2020; Received in revised form 14 August 2020; Accepted 13 September 2020
Available online 22 September 2020

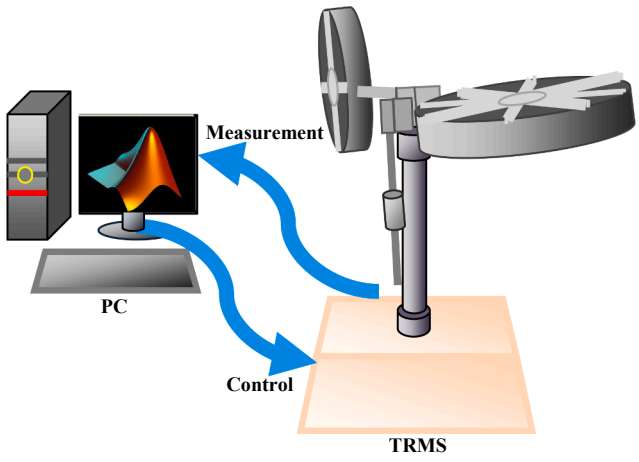

Fig. 1. TRMS configuration.

Table 1
Physical parameters of TRMS [27].

Symbol	Definition	Value
I_1	Moment of inertia of vertical rotor	6.8×10^{-2} kg·m^2
I_2	Moment of inertia of horizontal rotor	2×10^{-2} kg·m^2
a_1	Static characteristic parameter	0.0135
b_1	Static characteristic parameter	0.0924
a_2	Static characteristic parameter	0.02
b_2	Static characteristic parameter	0.09
M_g	Gravity momentum	0.32
$B_{1\psi}$	Friction momentum parameter	6×10^{-3} N·m·s/rad
$B_{1\varphi}$	Friction momentum parameter	1×10^{-1} N·m·s/rad
K_{gy}	Gyroscopic momentum parameter	0.05 s/rad
K_{gx}	Gyroscopic momentum parameter	0.0163 s/rad
k_{11}	Motor 1 gain	1.1
k_{22}	Motor 2 gain	0.8
T_{11}	Motor 1 denominator parameter	1.2
T_{10}	Motor 1 denominator parameter	1
T_{22}	Motor 2 denominator parameter	1
T_{20}	Motor 2 denominator parameter	1
T_p	Cross reaction momentum parameter	2
T_0	Cross reaction momentum parameter	3.5
k_c	Cross reaction momentum gain	−0.2

dynamic performance, an efficient method is to use nonlinear sliding surfaces. Global fast dynamic terminal sliding mode is one of the nonlinear sliding surfaces, which can make system states arrive at the equilibrium point along the sliding surface in a shorter time. Unfortunately, in the GFDTSMC the computing equivalent control needs the exact knowledge of the dynamic model, the proposed ARBFNNGFDTSMC is based on RBFNN, which is utilized to estimate the equivalent control of the GFDTSMC where only five radial basis functions are required for this control system and their weightings can be established and updated continuously by on-line learning algorithms are derived by using Lyapunov stability analysis.

Motivated by the previous researches, this paper proposes an ARBFNNGFDTSMC to overcome the uncertainties, external disturbances, and coupling effects for TRMS, where the adaptive RBFNN has been utilized in the developed controller so as to identified unknown nonlinear dynamics of the TRMS, consequently, another robust adjustment has been presented in the developed control synthesis, to compensate the estimation errors and to diminish the external disturbance effects. Stability analysis in the closed-loop has been proved using the Lyapunov method. In summary, the main contributions of this paper are highlighted by:

1. An adaptive RBFNN has been exploited in the developed controller design to identified unknown nonlinear dynamics of the TRMS. In addition, another adaptive control expressions has been added to diminish the wind gusts, external disturbance effects, and to compensate the estimation errors of the adaptive RBFNN.
2. The stability analysis in the closed-loop has been demonstrated by using Lyapunov method where all adjustment laws have been provided.
3. The developed ARBFNNGFDTSMC has been validated in practical experimentation.

Compared with the existing works [13,14,21–26], the contributions of this work can be summarized by:

- In [21], a robust backstepping controller based on the neuro adaptive observer for the TRMS is designed and implemented in real time, where the nonlinearities of the TRMS are estimated using Chebyshev neural network. A tuning scheme based on Lyapunov theory stability is developed which can guarantee the boundedness of tracking error. Unfortunately, this approach requires a complicate non-linear observer, which will increase the complication and calculation time. On the other hand, In this work, a robust ARBFNNGFDTSMC has been proposed without needing a non-linear observer where the unknown nonlinearities are approximated by the RBFNN whose weight value parameters are adjusted on-line according to some adaptive laws. The purpose of controlling the nonlinear system output is to track a given trajectory. Based on the RBF model, the Lyapunov synthesis approach is used to develop an adaptive control algorithm.
- The authors in [14], developed an adaptive high order sliding mode control for TRMS where the mathematical model of the TRMS is pseudo decoupled into horizontal subsystem and vertical subsystem. The cross-coupling effect between the main rotor and the tail rotor is considered as the uncertainty in the pseudo decoupled TRMS. An adaptive tuning law is realized to deal with system uncertainty. In addition, a proportional integral (PI) sliding surface is designed for the vertical subsystem in order to remove the offset in the pitch angle. The simulation results proved that this control technique can diminish the chattering phenomenon, but needs the knowledge of the sliding surfaces and its derivatives, moreover it is very sensible to noise measurement. This control strategy has been performed only in simulation without any experimental validation. In this work the proposed control has been designed without needing the decoupling procedure and without knowledge of the mathematical model of TRMS, where the adaptive neural network based on radial basis functions (RBF) is used to estimate the equivalent control, the adaptive learning algorithms are derived by using Lyapunov stability analysis. Furthermore, a novel global fast terminal sliding mode controller is designed by employing the proposed reaching law and sliding surface, which can quicken the convergence rate of the system states in both the reaching phase and the sliding phase. Theoretical analysis shows that the proposed controller can guaranty the Lyapunov stability. In addition, practical experimentation results are presented to verify the effectiveness of the proposed ARBFNNGFDTSMC.
- In [22], multistage feedback linearization control methodology has been developed for TRMS, where the coupling effects are maintained in controller derivation, there is no need to decouple the TRMS into horizontal and vertical subsystems. Exponential stability of the closed loop is guaranteed by using the second method of Lyapunov.

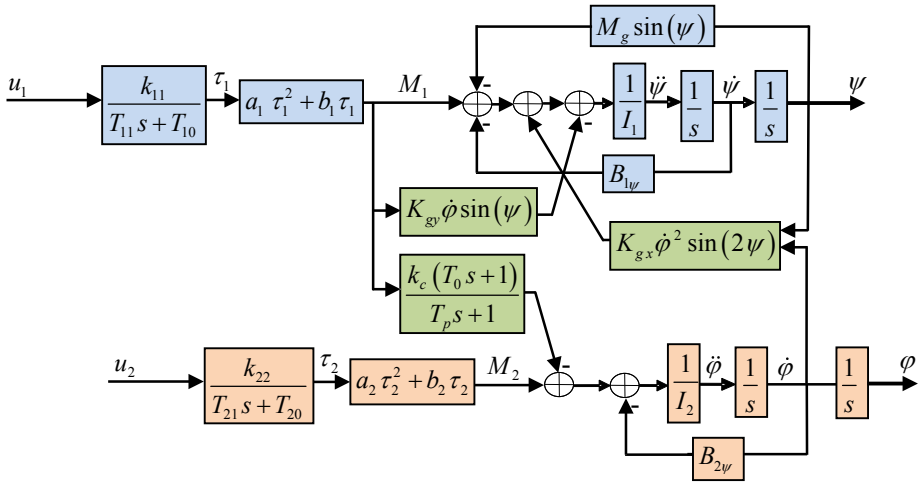

Fig. 2. Scheme of the TRMS.

To show the performance and the effectiveness of the proposed controller, simulation results are presented without considering the practical implementation, the results show a good tracking performance. Unfortunately, this control method is sensible to external disturbances. In addition, this control method requires a complicate non-linear observer to estimate the unmeasured states which increase the intricacy of the controller. On the other hand in this paper a robust ARBFNNGFDTSMC strategy has been investigated without needing a non-linear observer where a global fast terminal sliding mode controller is developed. With the introduction of the nonlinear function in the design of the sliding hyperplane, which assures the system tracking error convergence to zero in finite time. Furthermore, The output of the RBNN is used to compute the equivalent control, The proposed system stability is proved by Lyapunov analysis. On the other hand in this paper, practical experimentation of the proposed control strategy has been performed to the real TRMS.

- In [23], the authors proposed PID controllers with independent input for TRMS. In order to reduce total error and control energy, all parameters of the controller are obtained by a real-value-type genetic algorithm with a system performance index as the fitness function. In [24] a fuzzy PID control scheme with a real-valued genetic algorithm to control the TRMS to move quickly and accurately to the desired attitudes, both the pitch angle and the azimuth angle in a cross-coupled condition, a fuzzy compensator is applied to the PID controller. The proposed control structure includes PID controllers with independent inputs in 2-DOF. In order to reduce total error and control energy, all parameters of the controller are obtained by a real-valued genetic algorithm with the system performance index as a fitness function. The system performance index utilized the integral of time multiplied by the square error criterion to build a suitable fitness function in the real-valued genetic algorithm. In the control strategy proposed in [23,24], the stability analysis is not thoroughly proved. In this paper an ARBFNNGFDTSMC is used to achieves fast transient response, finite-time convergence and elevates control precision. In the proposed control strategy an exponential tracking error convergence of the TRMS is demonstrated by utilizing Lyapunov theory in its coupled configuration. Besides, the proposed control method does not needed decoupling stage.
- A fuzzy sliding mode control for the TRMS has been developed in [13] to decrease the chattering effect, notwithstanding good obtained results but there lacks the experimental validation. In this work an adaptive RBFNN has been used in the proposed controller design in order to estimate the equivalent control and unknown nonlinear dynamics of the TRMS due to uncertainties and external disturbances effects, In addition, another adaptive control term has been introduced to reduce the external disturbance effects and to compensate the approximation errors of the adaptive RBFNN system. In addition a practical experimentation of the proposed control has been effectuated to the real TRMS.

- A new control algorithm using model predictive control for TRMS has been proposed in [25], Another adaptive feedback linearization control strategy has been developed to the TRMS in [26], in order to achieve robust trajectory tracking, this two control strategies has been validated in real time implementation without taking into account the wind effects. Contrariwise, in this work, an ARBFNNGFDTSMC has been designed, where the proposed fast nonlinear terminal sliding surface can give a fast transient response, finite-time convergence without singularities problem, and strong robustness against wind effects.

According to the cited precedent papers, this paper elaborates an adaptive global fast dynamic terminal sliding mode control method in presence of wind effects where the developed control algorithm include a RBFNN and adaptive control in order to get a good trajectory following of TRMS, in addition stability analysis has been proved by using Laypunov method. So as to exhibit ability of the developed control method, practical experimentation is performed to the real TRMS prototype. The proposed control algorithm permit to avoid the modeling problems, to furnish a best robustness and to obtain a desired trajectory following with better accuracy in presence of wind effects. The proposed control strategy has several advantages such as:

- The knowledge of dynamic model of TRMS is not required in the control design;

– A strong performances in the presence of external disturbances and uncertainties;
– Achieves fast transient response, finite-time convergence and elevates control precision;
– The system stability is guaranteed by using Lyapunov method.
and the main disadvantages of the proposed control
– There is no specific rule for determining the RBFNN structure. The appropriate structure is achieved through experience and trial and error.
– Require huge processing time for large neural networks.

The rest of paper is arranged as follows, in Section 2, the TRMS description with dynamic modelling are adopted. Section 3 presents ARBFNNGFDTSMC design, experiment results are provided in Section 4. Section 5 presents performance comparison. Finally, conclusions are given in Section 6.

Abbreviations

RBFNN	Radial Basis Function Neural Network
ARBFNNGFDTSMC	Adaptive RBFNN Global Fast Dynamic Terminal Sliding Mode Control
RBF	Radial Basis Functions
MIMO	Multi Inputs Multi outputs
TRMS	Twin Rotor MIMO System
LQR	Linear Quadratic Regulator
PID	Proportional Integral Derivative
SMC	Sliding Mode control
GFDTSMC	Global Fast Dynamic Terminal Sliding Mode Control
CSMC	Classical Sliding Mode Control

2. TRMS description

As delineated in Fig. 1, the TRMS is an aero-dynamical system, its behavior is like of helicopter formed by two perpendicular rotors incited by DC motors, main rotor and tail rotor that are put on a beam which is contains counter weight. The main rotor produces a hoist force allowing the beam to turn in main or vertical plane (pitch angle noted ψ), while the tail rotor allows the beam to turn in tail or horizontal plane (yaw angle noted φ). The two rotors are controlled by varying the voltage of the DC motors. The main and tail angles measures are obtained by using position sensors placed in the pivot. The TRMS is a multi-variable system which is described by complex dynamics, high nonlinearities, and cross coupling. The system is controlled by using PC (personal computer) and the controller can be implemented in Matlab-Simulink environment of the interfacing computer to control the real system. The measured and control signals are transmitted by Advantech PCI-1711 card. The physical parameters are presented in Table.1.

2.1. Dynamic model of TRMS

The dynamic model of the TRMS is given in [27] by utilizing Newton-Euler method expressed as:

$$\begin{cases} \ddot{\psi} = \dfrac{1}{I_1}\left\{ -M_g sin(\psi) - B_{1\psi}\dot{\psi} + k_{gx}\dot{\varphi}^2 sin(2\psi) - \left(a_1\tau_1^2 + b_1\tau_1\right)\left(k_{gy}\dot{\varphi}cos(\psi) + 1\right) + w_1 \right\} \\ \ddot{\varphi} = \dfrac{1}{I_2}\left\{ -B_{1\varphi}\dot{\varphi} - \dfrac{k_c(T_0 s + 1)}{T_p s + 1}\left(a_1\tau_1^2 + b_1\tau_1\right) + a_2\tau_2^2 + b_2\tau_2 + w_2 \right\} \end{cases} \tag{1}$$

where: w_1 and w_2 are the wind effects.

The scheme of the TRMS is portrayed in Fig. 2, where unmistakably shows the strong cross-coupling effects and dynamic complexity of the system.

3. ARBFNNGFDTSMC design

The dynamic model in (1) can be rewritten in the state-space form, where the state vector is chossen as:

$$x = [x_1, x_2, x_3, x_4, x_5, x_6] = [\psi, \dot{\psi}, \varphi, \dot{\varphi}, \tau_1, \tau_2]^T \tag{2}$$

$$\begin{cases} \dot{x}_1 = x_2 \\ \dot{x}_2 = -\dfrac{M_g}{I_1} sin(x_1) - \dfrac{B_{1\psi}}{I_1} x_2 + \dfrac{K_{gx}}{I_1} x_4^2 sin(2 x_1) + \dfrac{a_1}{I_1} x_5^2 + \dfrac{b_1}{I_1} x_5 \left(1 - K_{gy} x_4 cos(x_1)\right) + w_1 \\ \dot{x}_3 = x_4 \\ \dot{x}_4 = -\dfrac{B_{1\varphi}}{I_2} x_4 - \dfrac{M_R}{I_2} + \dfrac{a_2}{I_2} x_6^2 + \dfrac{b_2}{I_2} x_6 + w_2 \\ \dot{x}_5 = -\dfrac{T_{10}}{T_{11}} x_5 + \dfrac{k_{11}}{T_{11}} u_1 \\ \dot{x}_6 = -\dfrac{T_{20}}{T_{22}} x_6 + \dfrac{k_{22}}{T_{22}} u_2 \end{cases} \tag{3}$$

The state space model (3) can be rearranged as:

$$\begin{cases} \dot{x}_1 = x_2 \\ \dot{x}_2 = f_{v1} + \alpha_1 x_5^2 + \alpha_2 x_5 f_{v2} + w_1 \\ \dot{x}_3 = x_4 \\ \dot{x}_4 = f_{h1} + \alpha_3 x_6^2 + \alpha_4 x_6 + w_2 \\ \dot{x}_5 = \alpha_5 x_5 + \alpha_6 u_1 \\ \dot{x}_6 = \alpha_7 x_6 + \alpha_8 u_2 \end{cases} \tag{4}$$

where:

$$f_{v1} = -\frac{M_g}{I_1} sin(x_1) - \frac{B_{1\psi}}{I_1} x_2 + \frac{K_{gx}}{I_1} x_4^2 sin(2 x_1)$$

$$\alpha_1 = \tfrac{a_1}{I_1},\ \alpha_2 = \tfrac{b_1}{I_1},\ f_{v2} = 1 - K_{gy} x_4 cos(x_1)$$

$$f_{h1} = -\tfrac{B_{1\varphi}}{I_2} x_4 - \tfrac{M_R}{I_2},\ \alpha_3 = \tfrac{a_2}{I_2},\ \alpha_4 = \tfrac{b_2}{I_2}$$

$\alpha_5 = -\frac{T_{10}}{T_{11}}, \alpha_6 = \frac{k_{11}}{T_{11}}, \alpha_7 = -\frac{T_{20}}{T_{22}}, \alpha_8 = \frac{k_{22}}{T_{22}}$

The tracking errors variables are defined by:

$$e_1 = \psi_d - x_1 \tag{5}$$

$$e_2 = \varphi_d - x_3 \tag{6}$$

The global fast dynamic terminal sliding surfaces are defined by [28–30]:

$$s_1 = \left(\lambda_1 + \frac{d}{dt}\right)^{r-1} e_1 + \beta_1 \, e_1^{m_1/n_1} \tag{7}$$

$$s_2 = \left(\lambda_2 + \frac{d}{dt}\right)^{r-1} e_2 + \beta_2 \, e_2^{m_2/n_2} \tag{8}$$

where: r is the relative degree of the system, $\lambda_1, \lambda_2, \beta_1, \beta_2, m_1, m_2, n_1$ and n_2 are positive constants with $m_1 < n_1$ and $m_2 < n_2$.

The relative degree of the TRMS is $r = 3$, thus:

$$s_1 = \ddot{e}_1 + 2\lambda_1 \dot{e}_1 + \lambda_1^2 e_1 + \beta_1 e_1^{m_1/n_1} \tag{9}$$

$$s_2 = \ddot{e}_2 + 2\lambda_2 \dot{e}_2 + \lambda_2^2 e_2 + \beta_2 e_2^{m_2/n_2} \tag{10}$$

The time derivative of (9) and (10) are calculated as:

$$\dot{s}_1 = \dddot{\psi}_d - F_{v1} - \alpha_5 x_5 F_{v2} - \alpha_6 F_{v2} u_1 - \alpha_2 x_5 F_{v3} - \dot{w}_1 + 2\lambda_1 \left(\ddot{\psi}_d - f_{v1} - \alpha_1 x_5^2 - \alpha_2 x_5 f_{v2} - w_1\right) + \left(\lambda_1^2 + \beta_1 \frac{m_1}{n_1} e_1^{\frac{m_1-n_1}{n_1}}\right)\left(\dot{\psi}_d - x_2\right) \tag{11}$$

$$\dot{s}_2 = \dddot{\varphi}_d - F_{h1} - \alpha_7 x_6 F_{h2} - \alpha_8 F_{h2} u_2 - \dot{w}_2 + 2\lambda_2 \left(\ddot{\varphi}_d - f_{h1} - \alpha_3 x_6^2 - \alpha_4 x_6 - w_2\right) + \left(\lambda_2^2 + \beta_2 \frac{m_2}{n_2} e_2^{\frac{m_2-n_2}{n_2}}\right)\left(\dot{\varphi}_d - x_4\right) \tag{12}$$

with:

$$F_{v1} = \frac{\partial f_{v1}}{\partial x_1} x_2 + \frac{\partial f_{v1}}{\partial x_2}\dot{x}_2 + \frac{\partial f_{v1}}{\partial x_4}\dot{x}_4$$

$$F_{v2} = 2\alpha_1 x_5 + \alpha_2 f_{v2}$$

$$F_{v3} = \frac{\partial f_{v2}}{\partial x_1} x_2 + \frac{\partial f_{v2}}{\partial x_4}\dot{x}_4$$

$$F_{h1} = \frac{\partial f_{h1}}{\partial x_4}\dot{x}_4 + \frac{\partial f_{h1}}{\partial x_5}\dot{x}_5$$

$$F_{h2} = 2\alpha_3 x_6 + \alpha_4$$

Let define the following Lyapunov function by:

$$V = \frac{1}{2} s_1^2 + \frac{1}{2} s_2^2 \tag{13}$$

The time derivative of (13) is given by:

$$\dot{V} = s_1 \dot{s}_1 + s_2 \dot{s}_2 \tag{14}$$

$$\dot{V} = s_1 \left[2\lambda_1 \left(\ddot{\psi}_d - f_{v1} - \alpha_1 x_5^2 - \alpha_2 x_5 f_{v2} - w_1\right) + \left(\lambda_1^2 + \beta_1 \frac{m_1}{n_1} e_1^{\frac{m_1-n_1}{n_1}}\right)\left(\dot{\psi}_d - x_2\right) + \dddot{\psi}_d - F_{v1} - \alpha_5 x_5 F_{v2} - \alpha_6 F_{v2} u_1 - \alpha_2 x_5 F_{v3} - \dot{w}_1\right] + s_2 \left[2\lambda_2 \left(\ddot{\varphi}_d - f_{h1} - \alpha_3 x_6^2 - \alpha_4 x_6 - w_2\right) + \left(\lambda_2^2 + \beta_2 \frac{m_2}{n_2} e_2^{\frac{m_2-n_2}{n_2}}\right)\left(\dot{\varphi}_d - x_4\right) + \dddot{\varphi}_d - F_{h1} - \alpha_8 F_{h2} u_2 - \dot{w}_2 - \alpha_7 x_6 F_{h2}\right] \tag{15}$$

The control laws u_1 and u_2 are given as:

$$u_1 = \frac{1}{\alpha_6 F_{v2}}\left[\dddot{\psi}_d - F_{v1} - \alpha_5 x_5 F_{v2} - \alpha_2 x_5 F_{v3} + 2\lambda_1 \left(\ddot{\psi}_d - f_{v1} - \alpha_1 x_5^2 - \alpha_2 x_5 f_{v2} - w_1\right) + \left(\lambda_1^2 + \beta_1 \frac{m_1}{n_1} e_1^{\frac{m_1-n_1}{n_1}}\right)\left(\dot{\psi}_d - x_2\right) - \dot{w}_1\right] + \mu_1 s_1 \tag{16}$$

$$u_2 = \frac{1}{\alpha_8 F_{h2}}\left[\dddot{\varphi}_d - F_{h1} - \alpha_7 x_6 F_{h2} + 2\lambda_2 \left(\ddot{\varphi}_d - f_{h1} - \alpha_3 x_6^2 - \alpha_4 x_6 - w_2\right) + \left(\lambda_2^2 + \beta_2 \frac{m_2}{n_2} e_2^{\frac{m_2-n_2}{n_2}}\right)\left(\dot{\varphi}_d - x_4\right) - \dot{w}_2\right] + \mu_2 s_2 \tag{17}$$

where: μ_1 and μ_2 positive constants.

Using (16) and (17), it can be cheeked that:

$$\dot{V} \leqslant -\mu_1 s_1^2 - \mu_2 s_2^2 < 0 \tag{18}$$

If we considered the absence of wind effects, i.e., $w_1 = \dot{w}_1 = w_2 = \dot{w}_2 = 0$, the ideal control laws are rearranged as:

$$u_1 = \frac{1}{\alpha_6 F_{v2}}\left[\dddot{\psi}_d - F_{v1} - \alpha_5 x_5 F_{v2} - \alpha_2 x_5 F_{v3} + 2\lambda_1 \left(\ddot{\psi}_d - f_{v1} - \alpha_1 x_5^2 - \alpha_2 x_5 f_{v2}\right) + \left(\lambda_1^2 + \beta_1 \frac{m_1}{n_1} e_1^{\frac{m_1-n_1}{n_1}}\right)\left(\dot{\psi}_d - x_2\right)\right] + \mu_1 s_1 \tag{19}$$

$$u_2 = \frac{1}{\alpha_8 F_{h2}}\left[\dddot{\varphi}_d - F_{h1} - \alpha_7 x_6 F_{h2} + 2\lambda_2 \left(\ddot{\varphi}_d - f_{h1} - \alpha_3 x_6^2 - \alpha_4 x_6\right) + \left(\lambda_2^2 + \beta_2 \frac{m_2}{n_2} e_2^{\frac{m_2-n_2}{n_2}}\right)\left(\dot{\varphi}_d - x_4\right)\right] + \mu_2 s_2 \tag{20}$$

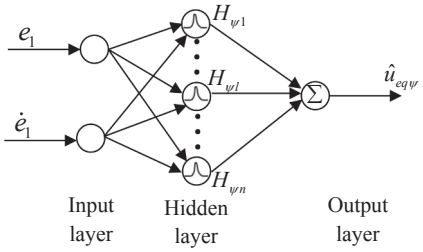

Fig. 3. RBFNN topology of the vertical subsystem.

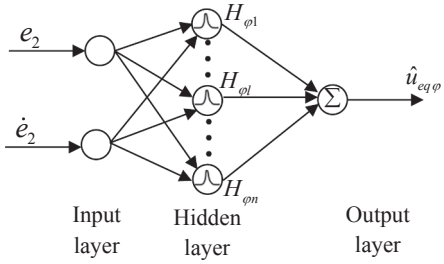

Fig. 4. RBFNN topology of the horizontal subsystem.

The functions $F_{vi}(i=1,2,3)$, $f_{vj}, F_{hj}(j=1,2)$ and $f_{h1}$are considered unknown and $w_1, \dot{w}_1, w_2$ and $\dot{w}_2$ expression which include wind effects are distinctive to zero, in this work an adaptive RBFNN has been utilized to solve this problem. The proposed control methodology concern the online identification of the ideal control laws u_1 and u_2 given in (19) and (20) by using RBFNN where the neural network weights are adjusted.

The ideal control laws u_1 and u_2, can be rewritten as [31]:

$$u_1 = u_{eq\ \psi} + \mu_1\ \ s_1 \tag{21}$$

$$u_2 = u_{eq\ \varphi} + \mu_2\ \ s_2 \tag{22}$$

where the equivalent controls $u_{eq\ \psi}$ and $u_{eq\ \varphi}$ are given by:

$$u_{eq\ \psi} = \frac{1}{\alpha_6\ F_{v2}}\left[\dddot{\psi}_d - F_{v1} - \alpha_5\ x_5 F_{v2} - \alpha_2\ x_5 F_{v3} + 2\lambda_1\ \left(\ddot{\psi}_d - f_{v1} - \alpha_1 x_5^2 - \alpha_2 x_5 f_{v2}\right) + \left(\lambda_1^{\ 2} + \beta_1\ \ \frac{m_1}{n_1}\ \ e_1^{\frac{m_1-n_1}{n_1}}\right)\left(\dot{\psi}_d - x_2\right)\right] \tag{23}$$

$$u_{eq\ \varphi} = \frac{1}{\alpha_8\ F_{h2}}\left[\dddot{\varphi}_d - F_{h1} - \alpha_7\ x_6 F_{h2} + 2\lambda_2\ \ \left(\ddot{\varphi}_d - f_{h1} - \alpha_3 x_6^2 - \alpha_4 x_6\right) + \left(\lambda_2^{\ 2} + \beta_2\ \ \frac{m_2}{n_2}\ \ e_2^{\frac{m_2-n_2}{n_2}}\right)\left(\dot{\varphi}_d - x_4\right)\right] \tag{24}$$

The equivalent controls u_{eq1} and u_{eq2} can be estimated by a RBFNN as:

$$\hat{u}_{eq\ \psi} = W_\psi^T\ H_\psi(x_\psi) \tag{25}$$

$$\hat{u}_{eq\ \varphi} = W_\varphi^T\ H_\varphi(x_\varphi) \tag{26}$$

where $H_\psi(x_\psi)$ and $H_\varphi(x_\varphi)$ are the Gaussian function of neural network, given by:

$$H_{\psi l} = G_\psi\left(\frac{\left(\|x_\psi - C_{\psi kl}\|^2\right)}{B_{\psi l}^{\ 2}}\right) \tag{27}$$

$$H_{\varphi l} = G_\varphi\left(\frac{\left(\|x_\varphi - C_{\varphi kl}\|^2\right)}{B_{\varphi l}^2}\right) \tag{28}$$

with: $x_\psi$and x_φ are the inputs the network, k is the input number of the network, l is the number of hidden layer nodes in the network, $H_\psi = [H_{\psi 1}\ H_{\psi 2}\ \ldots H_{\psi\ n}]^T$and $H_\varphi = [H_{\varphi 1}\ H_{\varphi 2}\ \ldots H_{\varphi\ n}]^T$ are the output of Gaussian function, $W_\psi$and W_φ are the neural network weights, the network input is chosen as $x_\psi = \left[e_1\ \dot{e}_1\right]^T$ and $x_\varphi = \left[e_2\ \dot{e}_2\right]^T$.

The topology of RBFNN are depicted in Fig. 3 and Fig. 4.

The real equivalent control laws $u_{eq\ \psi}$and $u_{eq\ \varphi}$is expired by:

$$u_{eq\ \psi} = W_\psi^{T^*} H_\psi(x_\psi) + \varepsilon_1 \tag{29}$$

$$u_{eq\ \varphi} = W_\varphi^{T^*} H_\varphi(x_\varphi) + \varepsilon_2 \tag{30}$$

where:ε_1 and $\varepsilon_2$are the estimation error that satisfy the condition:

$$\begin{cases} |\varepsilon_1| \leqslant \bar{\varepsilon}_1 \\ |\varepsilon_2| \leqslant \bar{\varepsilon}_2 \end{cases} \tag{31}$$

where: $W_\psi^{T^*}$, $W_\psi^{T^*}$are the optimal neural network weights and $\bar{\varepsilon}_1$and $\bar{\varepsilon}_2$are unknown positive parameters.

The estimated equivalent control laws $\hat{u}_{eq\ \psi}$and $\hat{u}_{eq\ \varphi}$is given as:

$$\hat{u}_{eq\ \psi} = W_\psi^T\ H_\psi(x_\psi) \tag{32}$$

$$\hat{u}_{eq\ \varphi} = W_\varphi^T\ H_\varphi(x_\varphi) \tag{33}$$

The ARBFNNGFDTSMC laws applied to the TRMS are expressed as [31]:

$$u_{\ 1} = \hat{u}_{eq\ \psi} + \hat{\varepsilon}_1\ \ tanh\left(\frac{s_1}{\chi_1}\right) + \mu_{\ 1}\ \ s_1 \tag{34}$$

$$u_2 = \hat{u}_{eq\varphi} + \hat{\varepsilon}_2 tanh\left(\frac{s_2}{\chi_2}\right) + \mu_2\ s_1 \tag{35}$$

where: χ_1, χ_2, μ_1 and $\mu_2$are designed positive constants.

By replacing (32) in (34) and (33) in (35), yields:

$$u_1 = W_\psi^T H_\psi(x_\psi) + \hat{\varepsilon}_1 tanh\left(\frac{s_1}{\chi_1}\right) + \mu_1 s_1 \tag{36}$$

$$u_2 = W_\varphi^T H_\varphi(x_\varphi) + \hat{\varepsilon}_2 tanh\left(\frac{s_2}{\chi_2}\right) + \mu_2 s_1 \tag{37}$$

W_ψ and $W_\varphi$weights are adjusted by:

$$\dot{W}_\psi = \gamma_1 s_1 H_\psi(x_\psi) - \sigma_1 W_\psi \tag{38}$$

$$\dot{W}_\varphi = \gamma_2 s_2 H_\varphi(x_\varphi) - \sigma_2 W_\varphi \tag{39}$$

where: $\gamma_1, \gamma_2, \sigma_1$ and $\sigma_2$are designed positive constants.

$\hat{\varepsilon}_1$ and $\hat{\varepsilon}_2$are adjusted by:

$$\dot{\hat{\varepsilon}}_1 = \eta_1\ \ s_1\ tanh\left(\frac{s_1}{\chi_1}\right) - \sigma_3\ \hat{\varepsilon}_1 \tag{40}$$

$$\dot{\hat{\varepsilon}}_2 = \eta_2\ \ s_2\ tanh\left(\frac{s_2}{\chi_2}\right) - \sigma_4\ \hat{\varepsilon}_2 \tag{41}$$

where: η_1, η_2, σ_3 and $\sigma_4$are designed positive constants.

3.1. Stability analysis

Let Define the following Lyapunov functions as:

$$V = \frac{1}{2}s_1^2 + \frac{1}{2}s_2^2 + \frac{1}{2\ \gamma_1}\tilde{W}_{\ \psi}^{\ T}\ \tilde{W}_\psi + \frac{1}{2\ \gamma_2}\tilde{W}_{\ \varphi}^{\ T}\ \tilde{W}_\varphi + + \frac{1}{2\ \eta_1}\tilde{\varepsilon}_1^T\ \ \tilde{\varepsilon}_1 + + \frac{1}{2\ \eta_2}\tilde{\varepsilon}_2^T\ \ \tilde{\varepsilon}_2 \tag{42}$$

where $\tilde{W}_\psi, \tilde{W}_\varphi, \tilde{\varepsilon}_1$and $\tilde{\varepsilon}_2$are the estimation errors defined by:

$$\tilde{W}_\psi^T = W_\psi^{T^*} - W_\psi^T \tag{43}$$

$$\tilde{W}_\varphi^T = W_\varphi^{T^*} - W_\varphi^T \tag{44}$$

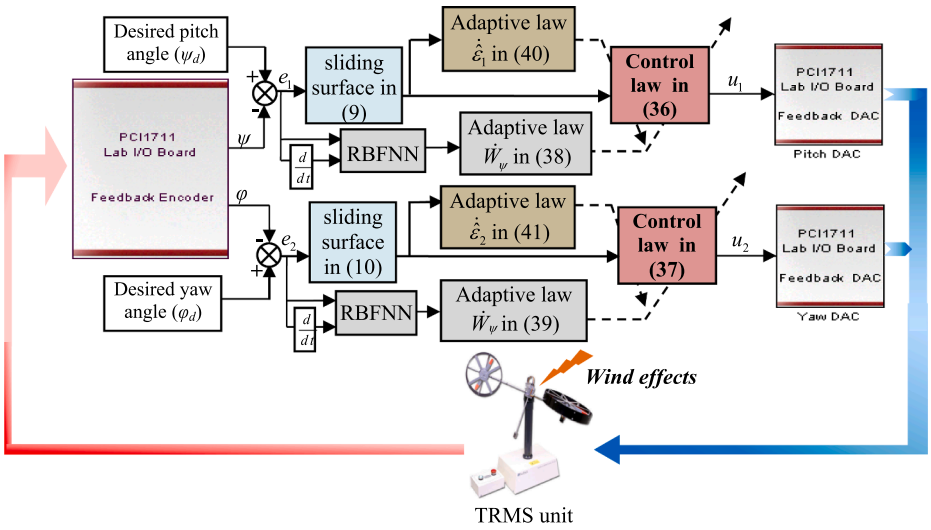

Fig. 5. Proposed ARBFNNGFDTSMC scheme.

$$\tilde{\varepsilon}_1 = \varepsilon_1^* - \hat{\varepsilon}_1 \tag{45}$$

$$\tilde{\varepsilon}_2 = \varepsilon_2^* - \hat{\varepsilon}_2 \tag{46}$$

The time derivative of (42) is given as:

By replacing (29), (30), (32) and (33) in (47) yields:

$$\dot{V} = s_1\ (u_{eq\ \psi} - u_1) + s_2\ (u_{eq\ \varphi} - u_2) + \frac{1}{\gamma_2}\tilde{W}_\varphi^T\ \dot{\tilde{W}}_\varphi + \frac{1}{\eta_1}\tilde{\varepsilon}_1^T\ \dot{\tilde{\varepsilon}}_1 + \frac{1}{\gamma_1}\tilde{W}_\psi^T\ \dot{\tilde{W}}_\psi + \frac{1}{\eta_2}\tilde{\varepsilon}_2^T\ \dot{\tilde{\varepsilon}}_2 \tag{47}$$

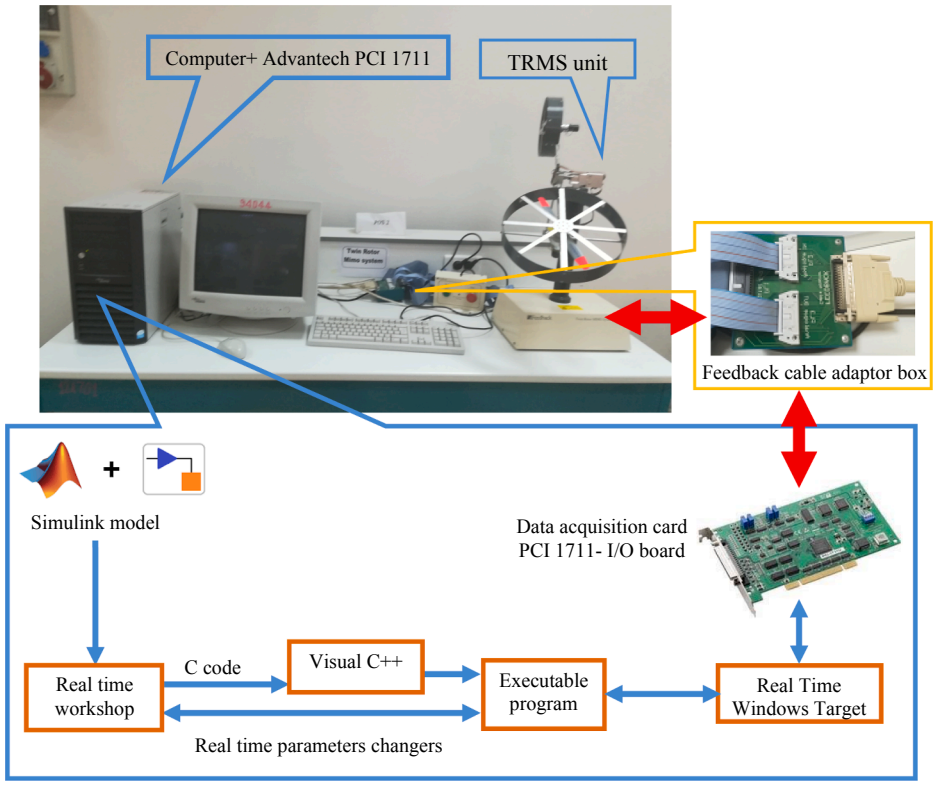

Fig. 6. Experimental configuration of the TRMS.

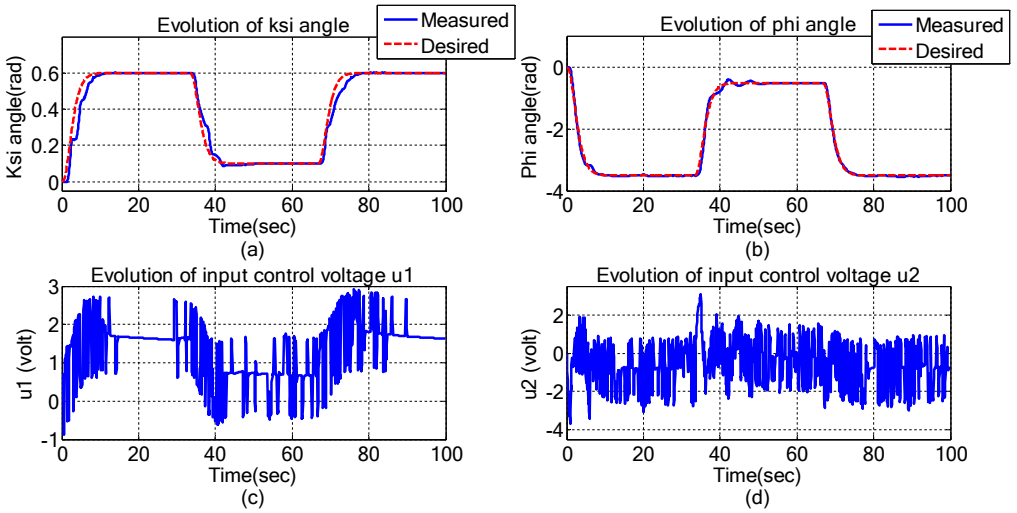

Fig. 7. Experimental results for square wave tracking.

$$\dot{V} \leqslant s_1 \left(W_\psi^{T^*} H_\psi(x_\psi) + \varepsilon_1 - W_\psi^T H_\psi(x_\psi) - \hat{\varepsilon}_1 \tanh\left(\frac{s_1}{\chi_1}\right) - \mu_1 s_1 \right) + \frac{1}{\gamma_1} \tilde{W}_\psi^T \dot{\tilde{W}}_\psi + \frac{1}{\eta_1} \tilde{\varepsilon}_1^T \dot{\tilde{\varepsilon}}_1$$

$$s_2 \left(W_\varphi^{T^*} H_\varphi(x_\varphi) + \varepsilon_2 - W_\varphi^T H_\varphi(x_\varphi) - \hat{\varepsilon}_2 \tanh\left(\frac{s_2}{\chi_2}\right) - \mu_2 s_2 \right) + \frac{1}{\gamma_2} \tilde{W}_\varphi^T \dot{\tilde{W}}_\varphi + \frac{1}{\eta_2} \tilde{\varepsilon}_2^T \dot{\tilde{\varepsilon}}_2 \quad (48)$$

The optimal parameters vector $W_\psi^{T^*}$ and $W_\varphi^{T^*}$ are slowly time varying,

$$\dot{\tilde{W}}_\psi = -\dot{W}_\psi \quad (49)$$

$$\dot{\tilde{W}}_\varphi = -\dot{W}_\varphi \quad (50)$$

$$\dot{\tilde{\varepsilon}}_1 = -\dot{\hat{\varepsilon}}_1 \quad (51)$$

$$\dot{\tilde{\varepsilon}}_2 = -\dot{\hat{\varepsilon}}_2 \quad (52)$$

Substituting (49), (50), (51) and (52) in (48) and taking account (43),(44),(45) and (46), then (48) is rewritten as:

$$\dot{V} \leqslant -\mu_1 s_1^2 - \mu_2 s_2^2 + s_1 \tilde{W}_\psi^T H_\psi(x_\psi) + s_2 \tilde{W}_\varphi^T H_\varphi(x_\varphi) + s_1 \left(\varepsilon_1 - \hat{\varepsilon}_1 \tanh\left(\frac{s_1}{\chi_1}\right) \right) + s_2 \left(\varepsilon_2 - \hat{\varepsilon}_2 \tanh\left(\frac{s_2}{\chi_2}\right) \right) - \ldots$$

thus the time derivative of estimation error will be:

$$\frac{1}{\gamma_1} \tilde{W}_\psi^T \dot{W}_\psi - \frac{1}{\eta_1} \tilde{\varepsilon}_1^T \dot{\hat{\varepsilon}}_1 - \frac{1}{\gamma_2} \tilde{W}_\varphi^T \dot{W}_\varphi - \frac{1}{\eta_2} \tilde{\varepsilon}_2^T \dot{\hat{\varepsilon}}_2 \quad (53)$$

By introducing (38), (39),(40) and (41) into (53), yields:

$$\dot{V} \leqslant -\mu_1 s_1^2 - \mu_2 s_2^2 + s_1 \left(\varepsilon_1 - \hat{\varepsilon}_1 \tanh\left(\frac{s_1}{\chi_1}\right) \right) + s_2 \left(\varepsilon_2 - \hat{\varepsilon}_2 \tanh\left(\frac{s_2}{\chi_2}\right) \right) + \frac{\sigma_1}{\gamma_1} \tilde{W}_\psi^T W_\psi + \frac{\sigma_2}{\gamma_2} \tilde{W}_\varphi^T W_\varphi + \frac{\sigma_3}{\eta_1} \tilde{\varepsilon}_1 \hat{\varepsilon}_1 - \ldots$$

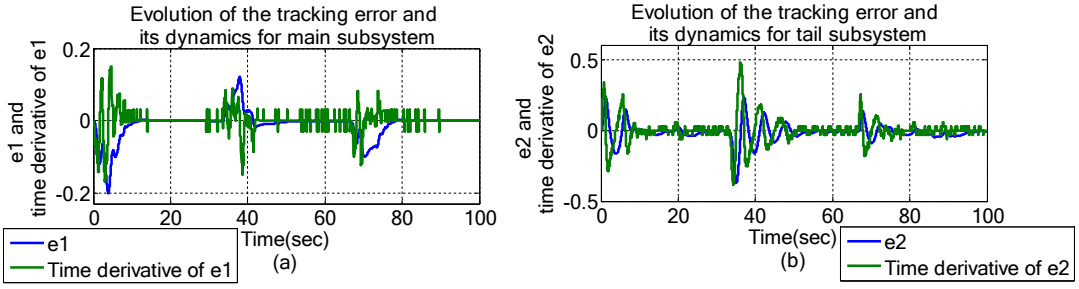

Fig. 8. Tracking error and it's dynamics for square wave tracking.

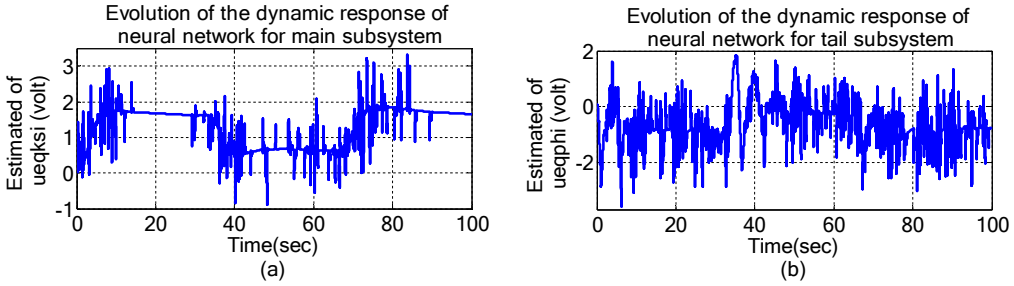

Fig. 9. Dynamic response of neural network for square wave tracking.

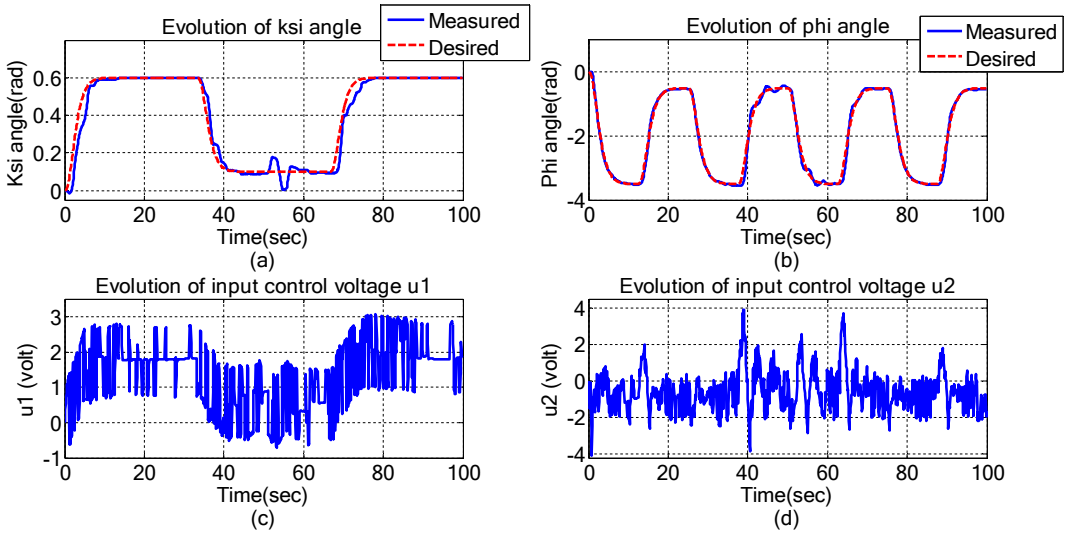

Fig. 10. Experimental results for square wave tracking with different frequencies.

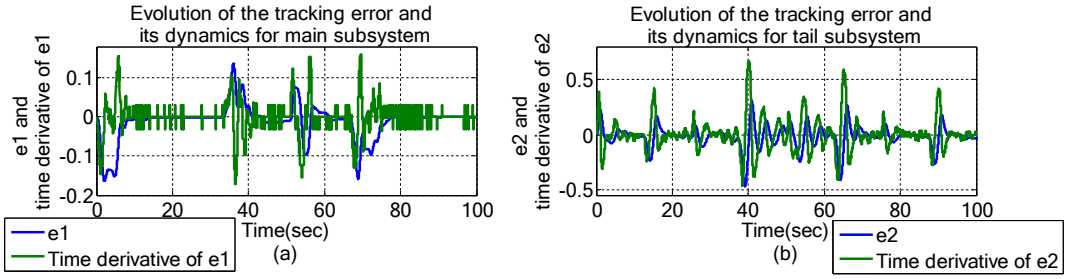

Fig. 11. Tracking error and it's dynamics for square wave tracking with different frequencies.

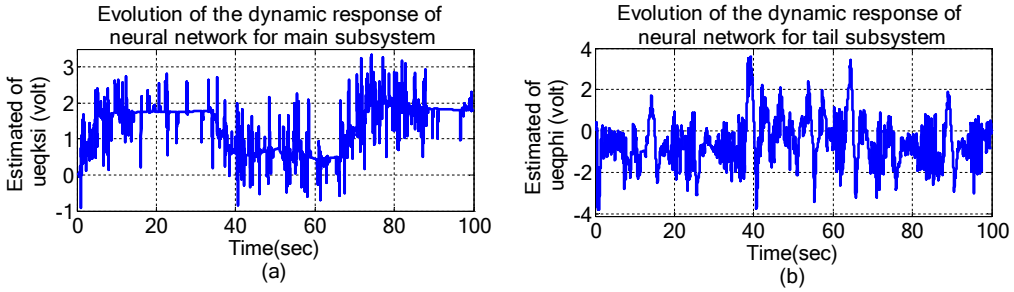

Fig. 12. Dynamic response of neural network for square wave tracking with different frequencies.

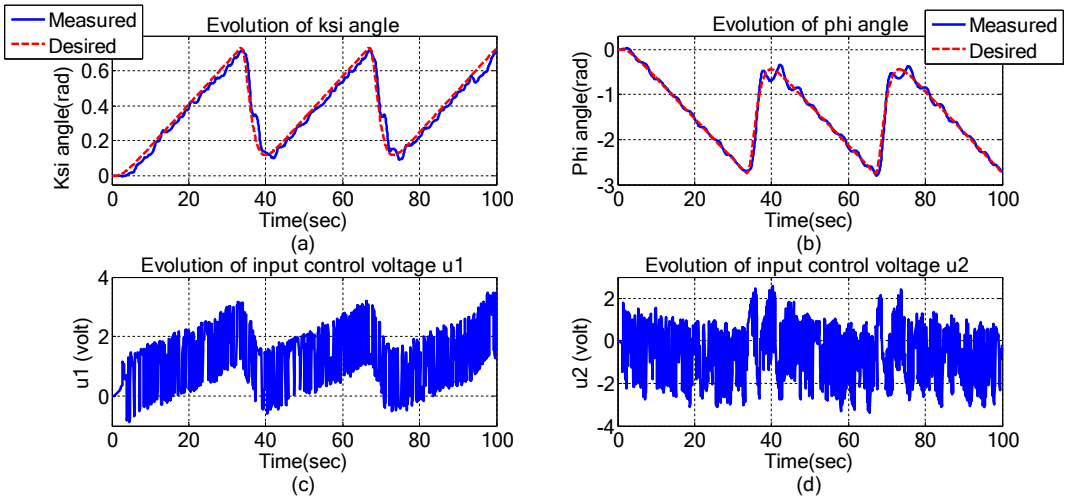

Fig. 13. Experimental results for triangle wave tracking.

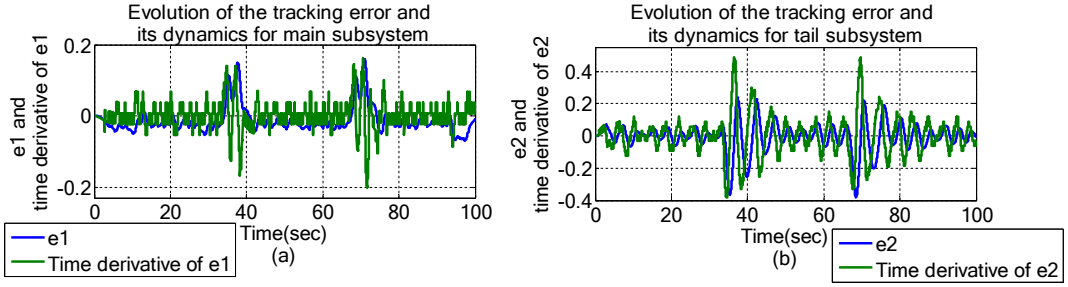

Fig. 14. Tracking error and it's dynamics for triangle wave tracking.

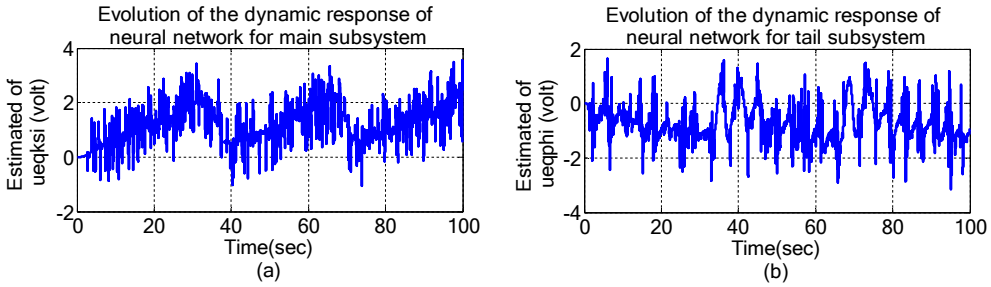

Fig. 15. Dynamic response of neural network for triangle wave tracking.

$$\frac{1}{\eta_1}\tilde{\varepsilon}_1\,\eta_1\,s_1\tanh\left(\frac{s_1}{\chi_1}\right)-\frac{1}{\eta_2}\tilde{\varepsilon}_2\,\eta_2\,s_2\tanh\left(\frac{s_2}{\chi_2}\right)+\frac{\sigma_4}{\eta_2}\tilde{\varepsilon}_2\,\hat{\varepsilon}_2 \tag{54}$$

Substituting (45), (46) in (54) we obtain:

$$\dot{V}\leqslant \quad -\mu_1 s_1^2-\mu_2 s_2^2+s_1\left(\varepsilon_1-\hat{\varepsilon}_1\tanh\left(\frac{s_1}{\chi_1}\right)\right)+s_2\left(\varepsilon_2-\hat{\varepsilon}_2\tanh\left(\frac{s_2}{\chi_2}\right)\right)+\frac{\sigma_1}{\gamma_1}\tilde{W}_\psi^T W_\psi-\varepsilon_1^* s_1\tanh\left(\frac{s_1}{\chi_1}\right)+\ldots$$

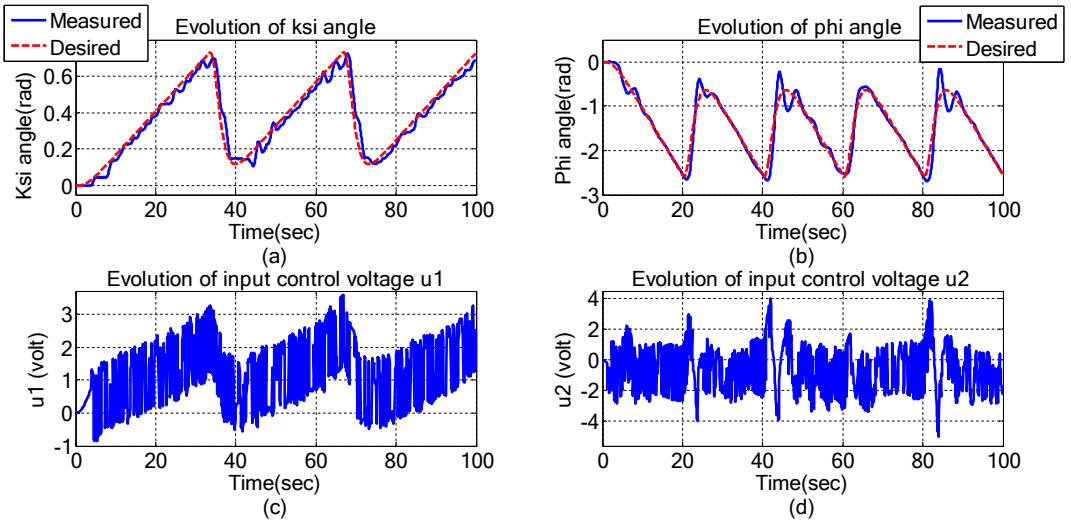

Fig. 16. Experimental results for triangle wave tracking with different frequencies.

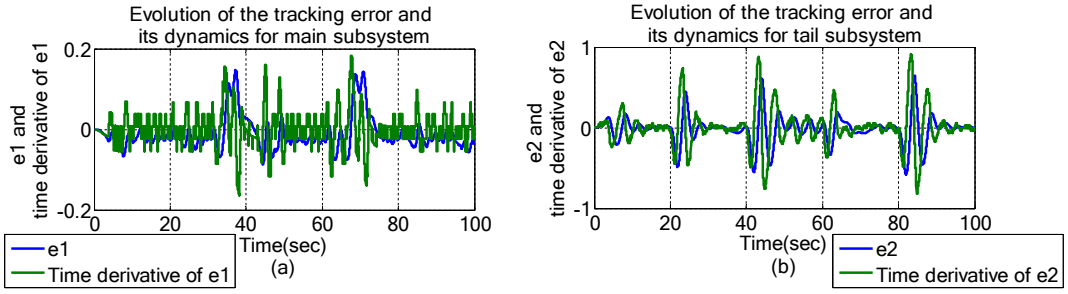

Fig. 17. Tracking error and it's dynamics for triangle wave tracking with different frequencies.

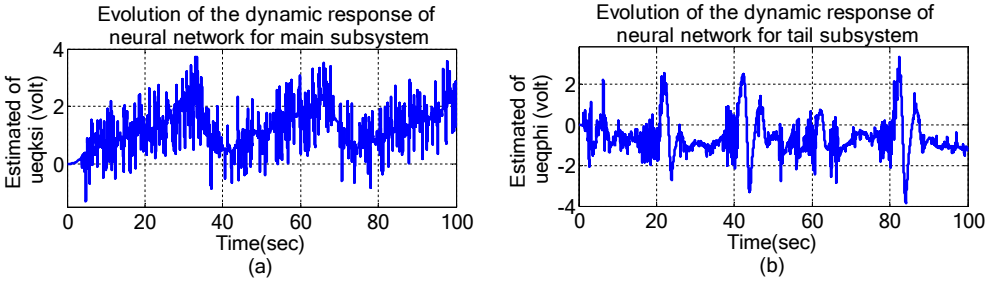

Fig. 18. Dynamic response of neural network for triangle wave tracking with different frequencies.

$$\hat{\varepsilon}_1 \quad s_1 \tanh\left(\frac{s_1}{\chi_1}\right) + \frac{\sigma_3}{\eta_1}\tilde{\varepsilon}_1 \quad \hat{\varepsilon}_1 + \frac{\sigma_2}{\gamma_2}\tilde{W}_{\varphi}^{T} \quad W_{\varphi} - \varepsilon_2^{*} \quad s_2 \tanh\left(\frac{s_2}{\chi_2}\right) + \hat{\varepsilon}_2 \quad s_2 \tanh\left(\frac{s_2}{\chi_2}\right) + \frac{\sigma_4}{\eta_2}\tilde{\varepsilon}_2 \quad \hat{\varepsilon}_2 \tag{55}$$

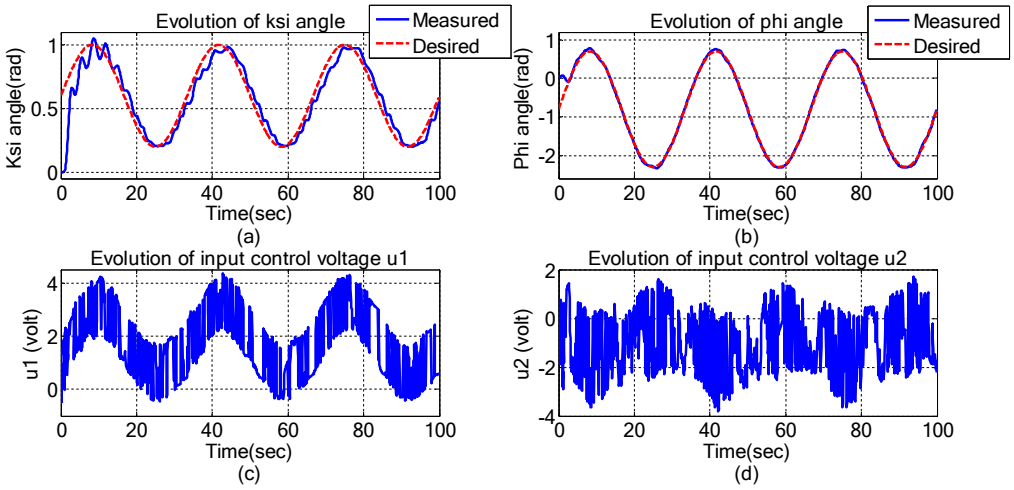

Fig. 19. Experimental results for sine wave tracking.

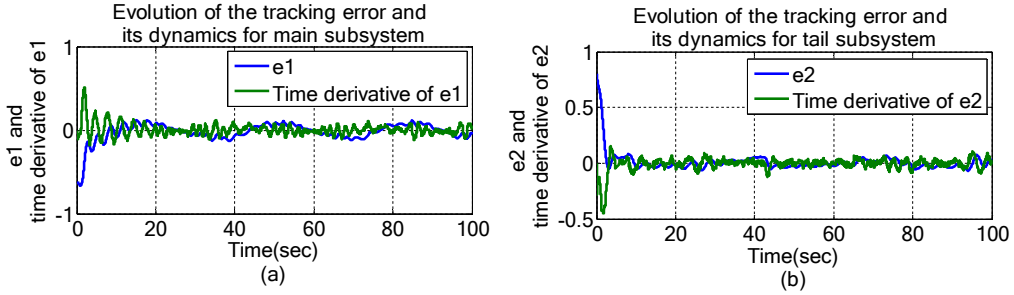

Fig. 20. Tracking error and it's dynamics for sine wave tracking.

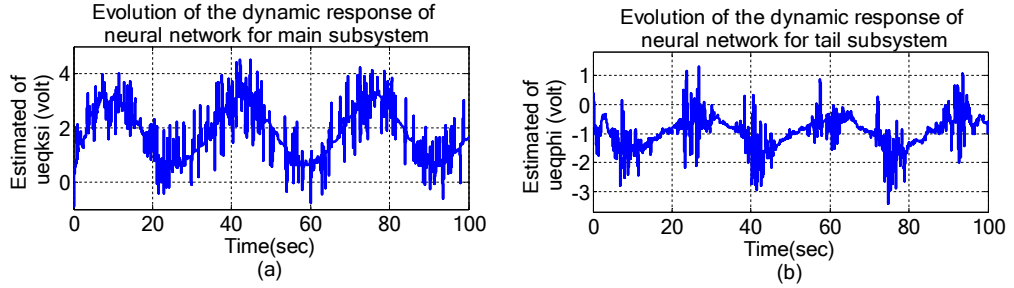

Fig. 21. Dynamic response of neural network for sine wave tracking.

Or equivalently:

$$\dot{V} \leqslant \quad -\mu_1 s_1^2 - \mu_2 s_2^2 + \frac{\sigma_1}{\gamma_1}\tilde{W}_\psi^T W_\psi - \varepsilon_1^* s_1 \tanh\left(\frac{s_1}{\chi_1}\right) + \frac{\sigma_3}{\eta_1}\tilde{\varepsilon}_1 \hat{\varepsilon}_1 + |s_1| \varepsilon_1^* + \frac{\sigma_2}{\gamma_2}\tilde{W}_\varphi^T W_\varphi - \varepsilon_2^* s_2 \tanh\left(\frac{s_2}{\chi_2}\right) + \ldots$$

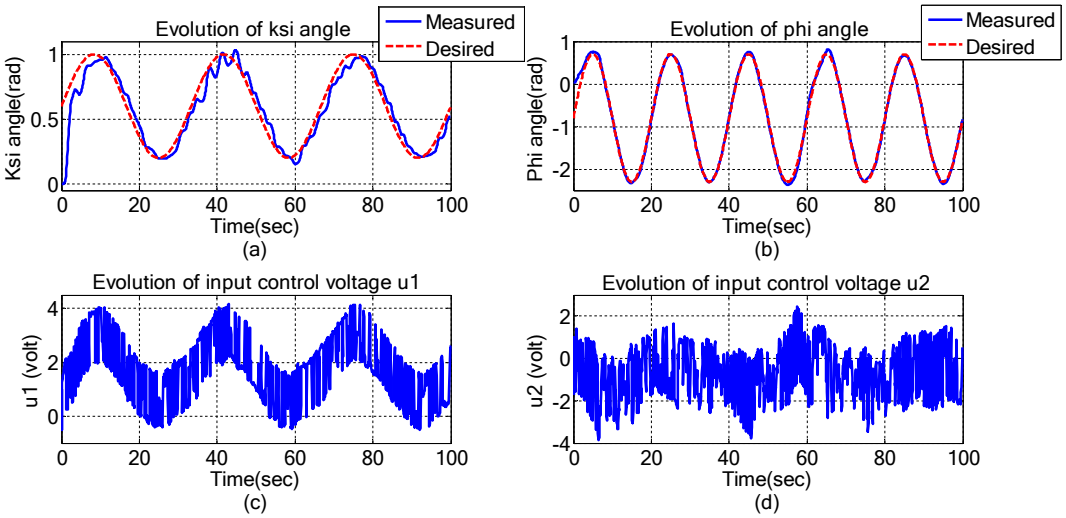

Fig. 22. Experimental results for sine wave tracking with different frequencies.

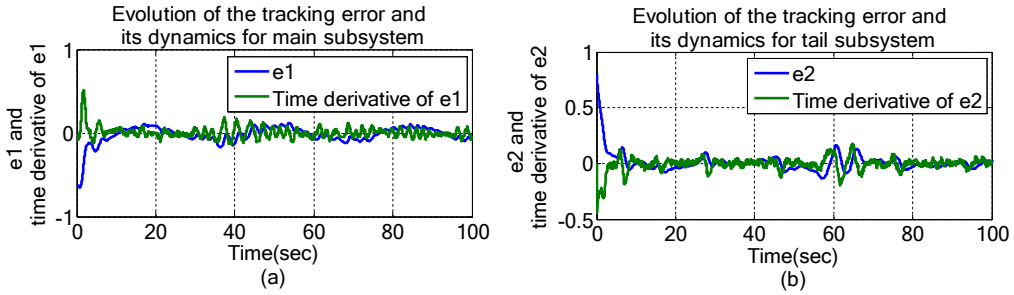

Fig. 23. Tracking error and it's dynamics for sine wave tracking with different frequencies.

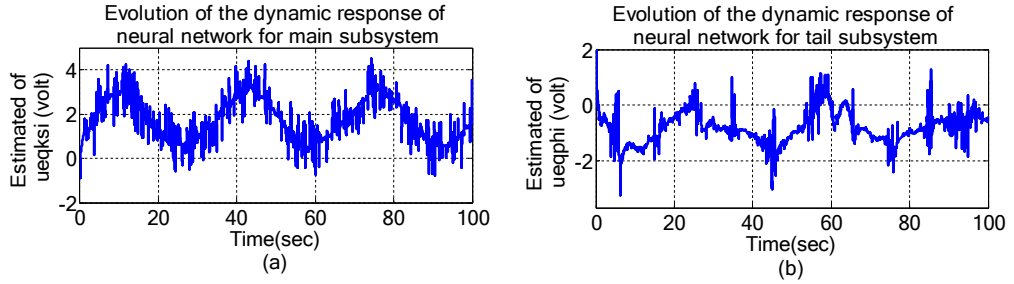

Fig. 24. Dynamic response of neural network for sine wave tracking with different frequencies.

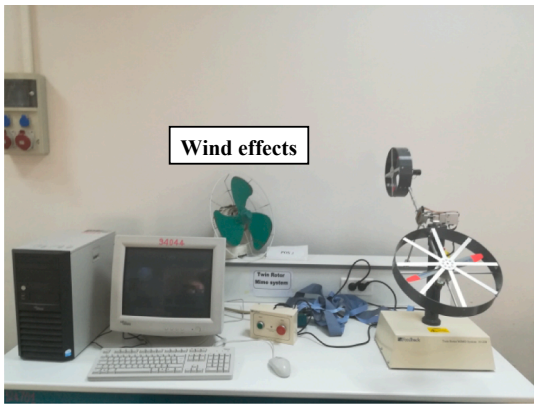

Fig. 25. Experimental workbench of the TRMS in presence wind effects.

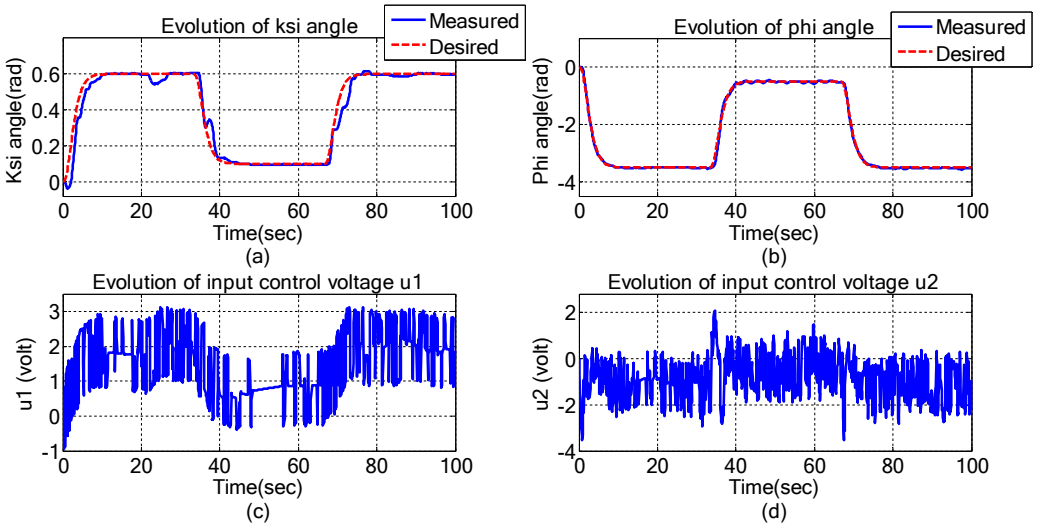

Fig. 26. Experimental results for square wave tracking in presence of wind effects.

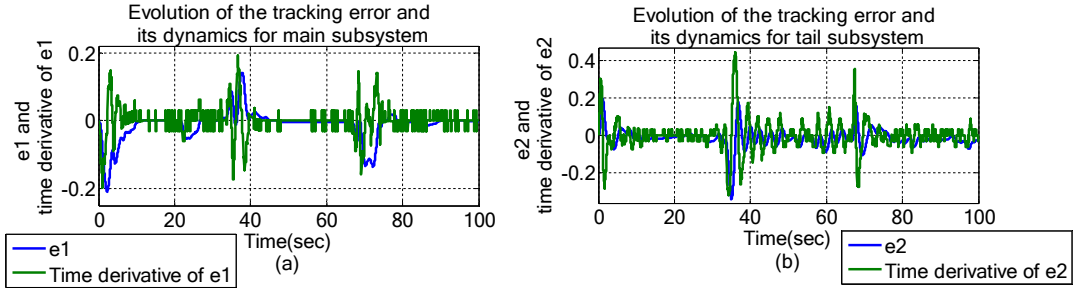

Fig. 27. Tracking error and it's dynamics for square wave tracking in presence of wind effects.

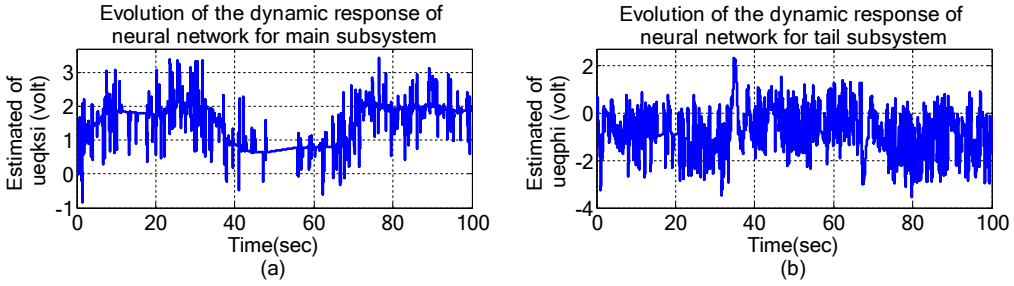

Fig. 28. Dynamic response of neural network for square wave tracking in presence of wind effects.

$$\frac{\sigma_4}{\eta_2}\tilde{\varepsilon}_2 \quad \widehat{\varepsilon}_2 + |s_2| \quad \varepsilon_2^* \tag{56}$$

Consider the inequality written as follows for any value of $\zeta > 0$ [32]:

$$|s| \quad - \quad s\tanh\left(\frac{s}{\chi}\right) \leqslant \zeta \quad \chi = \varsigma \tag{57}$$

with $\zeta$is a constant that verifies $\zeta = e^{-\ (\zeta+1)}$, i.e. $\zeta = 0.2785$.

(56) is rewritten as:

$$\dot{V} \leqslant \quad -\mu_1 s_1^2 - \mu_2 \quad s_2^2 + \varepsilon_1^* \varsigma_1 + \frac{\sigma_1}{\gamma_1}\tilde{W}_\psi^T \quad W_\psi \quad + \frac{\sigma_3}{\eta_1}\tilde{\varepsilon}_1 \quad \widehat{\varepsilon}_1 + \varepsilon_2^* \varsigma_2 + \frac{\sigma_2}{\gamma_2}\tilde{W}_\varphi^T \quad W_\varphi \quad + \frac{\sigma_4}{\eta_2}\tilde{\varepsilon}_2 \quad \widehat{\varepsilon}_2 \tag{58}$$

By utilizing young's inequality, one has:

$$\frac{\sigma_1}{\gamma_1}\tilde{W}_\psi^T \quad W_\psi \leqslant -\frac{\sigma_1}{2\gamma_1}\tilde{W}_\psi^T \quad W_\psi + \frac{\sigma_1}{2\gamma_1}\tilde{W}_\psi^{T^*} \quad W_\psi^* \tag{59}$$

$$\frac{\sigma_2}{\gamma_2}\tilde{W}_\varphi^T \quad W_\varphi \leqslant -\frac{\sigma_2}{2\gamma_2}\tilde{W}_\varphi^T \quad W_\varphi + \frac{\sigma_2}{2\gamma_2}\tilde{W}_\varphi^{T^*} \quad W_\varphi^* \tag{60}$$

$$\frac{\sigma_l}{\eta_j}\tilde{\varepsilon}_j^T \widehat{\varepsilon}_j \leqslant -\frac{\sigma_2}{2\eta_j}\tilde{\varepsilon}_j^2 + \frac{\sigma_2}{2\eta_j}\left|\varepsilon_j^*\right|^2, j = 1,2 \text{ and } l = 3,4 \tag{61}$$

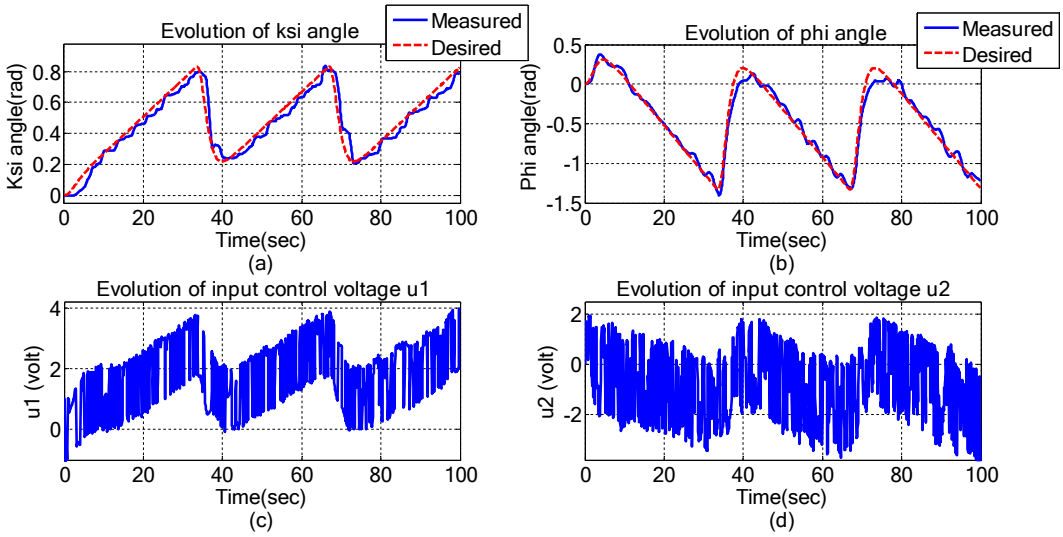

Fig. 29. Experimental results for triangle wave tracking in presence of wind effects.

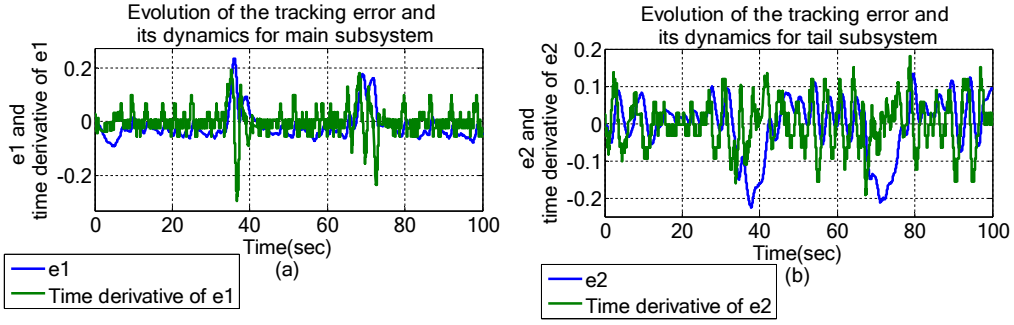

Fig. 30. Tracking error and it's dynamics for triangle wave tracking in presence of wind effects.

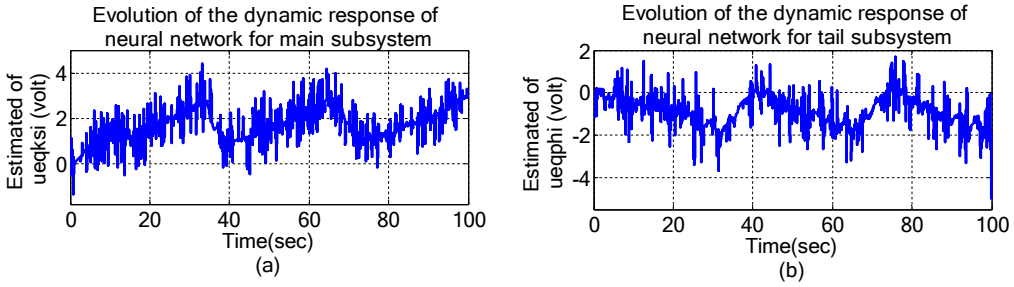

Fig. 31. Dynamic response of neural network for triangle wave tracking in presence of wind effects.

By introducing (59), (60) and (61) into (58), yields:

(58) becomes:

$$\dot{V} \leqslant \quad -\mu_1 s_1^2 - \mu_2 s_2^2 + \varepsilon_1^* \varsigma_1 - \frac{\sigma_1}{2\gamma_1} \tilde{W}_\psi^T W_\psi + \frac{\sigma_1}{2\gamma_1} \tilde{W}_\psi^{T^*} W_\psi^* - \frac{\sigma_3}{2\eta_1} \tilde{\varepsilon}_1^2 + \frac{\sigma_3}{2\eta_1} |\varepsilon_1^*|^2 + \varepsilon_2^* \varsigma_2 - \frac{\sigma_2}{2\gamma_2} \tilde{W}_\varphi^T W_\varphi + \frac{\sigma_2}{2\gamma_2} \tilde{W}_\varphi^{T^*} W_\varphi^* - \ldots - \frac{\sigma_4}{2\eta_2} \tilde{\varepsilon}_2^2 + \frac{\sigma_4}{2\eta_2} |\varepsilon_2^*|^2 \tag{62}$$

Let's specify:

$$c = min\{\sigma_1, \sigma_2, \sigma_3, \sigma_4, 2\mu_1, 2\mu_2\} \tag{63}$$

$$\dot{V} \leqslant -cV + \rho \tag{64}$$

With:

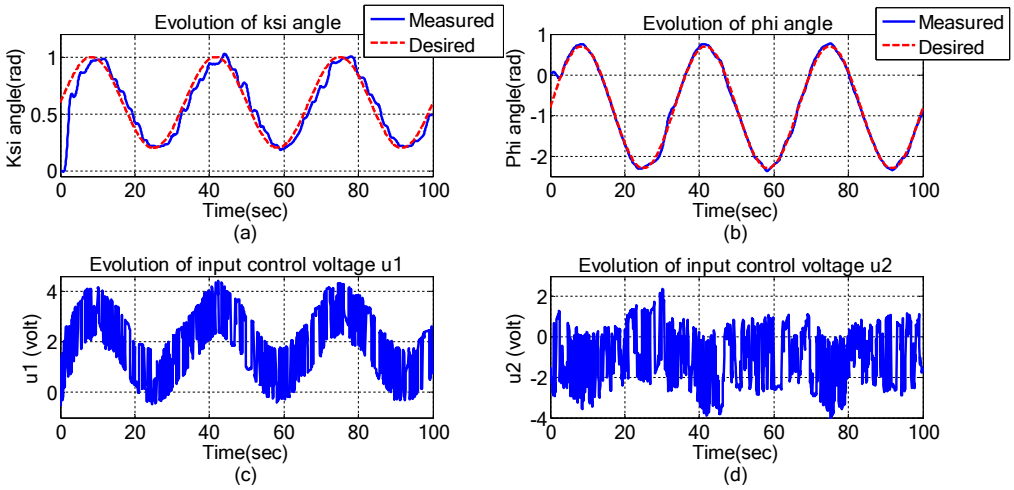

Fig. 32. Experimental results for sin wave tracking in presence of wind effects.

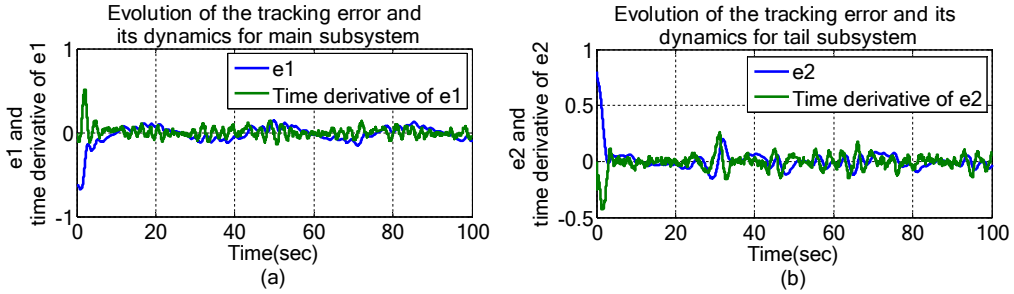

Fig. 33. Tracking error and it's dynamics for sin wave tracking in presence of wind effects.

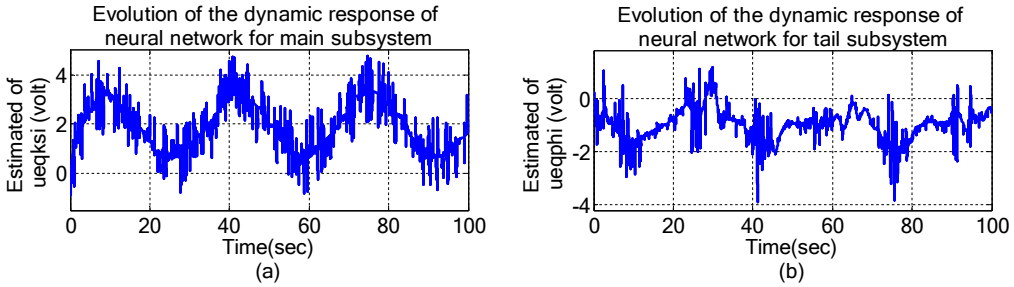

Fig. 34. Dynamic response of neural network sin wave tracking in presence of wind effects.

$$\rho = \varepsilon_1^* \varsigma_1 + \frac{\sigma_1}{2\gamma_1}\tilde{W}_\psi^{T^*} W_\psi^* + \frac{\sigma_3}{2\eta_1}\left|\varepsilon_1^*\right|^2 + \varepsilon_2^* \varsigma_2 + \frac{\sigma_2}{2\gamma_2}\tilde{W}_\varphi^{T^*} W_\varphi^* + \frac{\sigma_4}{2\eta_2}\left|\varepsilon_2^*\right|^2 \quad (65)$$

By Integrating (64), yields:

$$V(t) \leqslant V(0)\, e^{-ct} + \frac{\rho}{c} \quad (66)$$

From (64) it can be demonstrated that the developed control laws of TRMS presented in (36) and (37) are stable in spite of the presence of wind effects therefore the tracking errors converge to zero. In addition the weighting values of radial basis functions can be converged by on-line learning with zero initial weighting values. Adaptive training algorithm were derived in the sense of Lyapunov stability analysis as presented in (38) and (39), so that system-tracking stability of the closed-loop can be assured. The proposed control methodology is depicted in Fig. 5.

4. Experimental results

The experimental configuration of TRMS with personal computer (PC) is presented in Fig. 6. The TRMS comprises by five main components, 33-220 TRMS unit, PC, Advantech PCI 1711 card, feedback cable adaptor box and on/off switch box. The measures of main and tail angles of the beam ($\psi$and φ angles) are given by using digital encoders sensor. The measured angles are transmitted to the PC by using the interface unit. The voltages control inputs are transmitted to the TRMS, which lead the rotors. In this work, a PC (Intel(R) Core(TM) 3.00 GHz processor, 1 GB RAM) with 32-bit XP-Windows operating system and MATLAB/Simulink environment are used in order to implement in real time the developed control strategy.

The proposed controller was implemented using Simulink, a graphical programming language tool developed by MathWorks. The control design flow diagram is depicted in Fig. 6. The Simulink model is transferred to Real-Time Workshop (RTW) to build a C++ source program. C++ compiler compiles and links this program to produce an executable

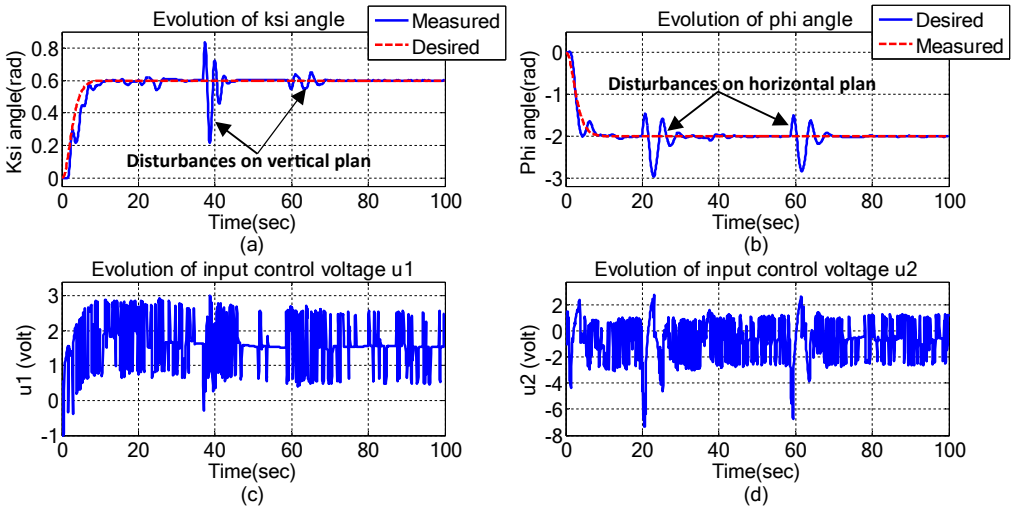

Fig. 35. Step responses of the TRMS with the proposed controller subject to the external disturbance.

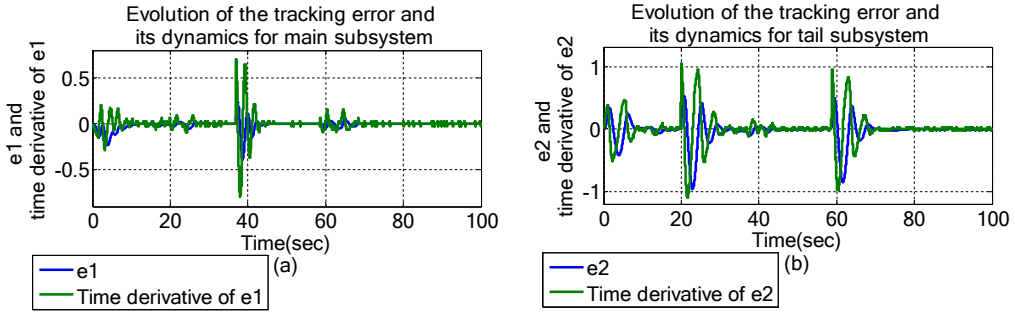

Fig. 36. Tracking error and it's dynamics for external disturbance rejection.

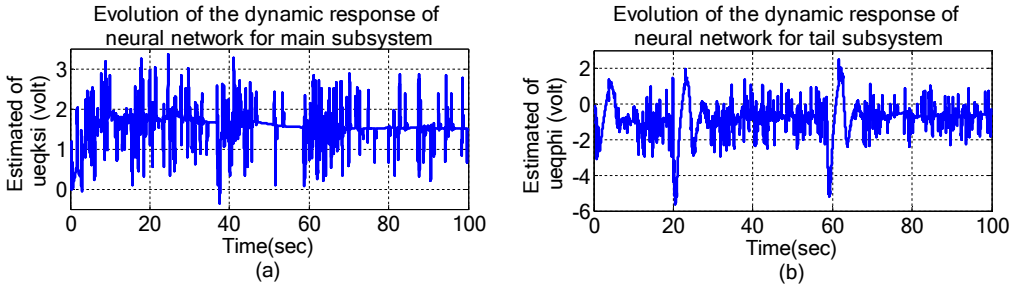

Fig. 37. Dynamic response of neural network for external disturbance rejection.

code. Real-Time Windows target is used as an interface between the created executable program acting as the control program and the input/output (I/O) board [27].

4.1. Test1: Square wave tracking

To treat the regulation mission of the TRMS, square reference trajectories has been considered for main and tail angles, the experimental results are depicted in Figs. 7 and Fig. 10, It is remarked that the developed control strategy is able to preserving the regulated positions as presented in Fig. 7(a and b). Fig. 8(a and b) represents the tracking error and it's dynamics of main and tail subsystems, the dynamic response of neural network for square wave tracking is depicted in Fig. 9 (a and b).

The pursuit responses of square reference trajectory, with different frequencies is carried out with experimentation as showed in Fig. 10(a and b) which demonstrates the capability of the proposed control algorithm to deals with diverse coupling of the two subsystems, after small transient perturbations in pitch and yaw angles responses as depicted in Fig. 10(a and b), due to the discontinuous nature of the square signals. The tracking error and it's dynamics of main and tail subsystems is presented in Fig. 11(a and b), the dynamic response of neural network is depicted in Fig. 12(a and b). The control input signals showed in (Fig. 7 (c and d) and Fig. 10(c and d)) are limited to the permit interval.

4.2. Test2: Triangle wave tracking

The efficiency of the proposed control method in experimentation with triangle reference trajectories are depicted in Fig. 13 and Fig. 16. The capability of the triangle trajectory following is confirmed in these figures. It is noted that trajectory tracking performances are demonstrated in practical implementation as presented in Fig. 13(a and b).

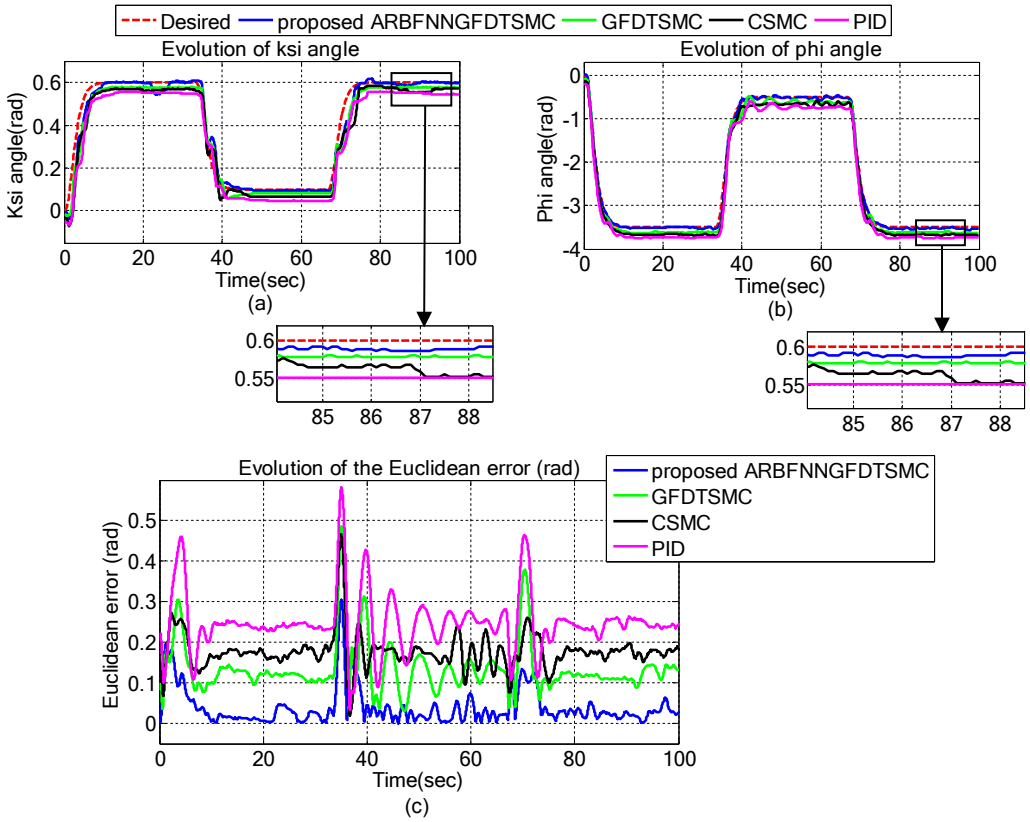

Fig. 38. Square wave tracking comparison between the proposed ARBFNNGFDTSMC, GFDTSMC, CSMC and PID control with wind effects.

Fig. 14(a and b) represents the tracking error and it's dynamics of main and tail subsystems, the dynamic response of neural network for triangle wave tracking is depicted in Fig. 15(a and b).

Fig. 16(a and b) indicates the effectuated trajectories by the TRMS with respect to triangle desired trajectory with different frequencies in experiment implementation, it is appear that the developed control strategy can overcome the coupling effects between the tail and main subsystems, after small overshoot in pitch and yaw angles responses as shown in (Fig. 10(a and b)) in reason to the nature of the triangle signals. The tracking error and it's dynamics of main and tail subsystems is presented in Fig. 17(a and b), the dynamic response of neural network is depicted in Fig. 18(a and b). The main and tail control input signals is depicted in (Fig. 13(c and d) and Fig. 16(c and d)) are bounded in the permit interval.

4.3. Test3: Sine wave tracking

The experiment results showed in Fig. 19 and Fig. 22 demonstrate the trajectory following responses of the TRMS according to sine reference signals for main and tail angles, the experimental results of main angle (ψ) and tail angle (φ) indicated in Fig. 19(a and b), demonstrate the capability of the proposed control method in the trajectory tracking problem.

Fig. 20(a and b) represents the tracking error and it's dynamics of main and tail subsystems, the dynamic response of neural network for sine wave tracking is depicted in Fig. 21(a and b).

In addition Fig. 22(a and b) present the effectuated trajectory by the TRMS, with respect to sine reference trajectory with different frequencies in experiment, to prove the efficiency of the proposed control methodology to deals with coupling effects between the two subsystems. The tracking error and it's dynamics of main and tail subsystems is presented in Fig. 23(a and b), the dynamic response of neural network is depicted in Fig. 24(a and b). The control input voltages as shown in Fig. 19(c and d) and Fig. 22(c and d) for main and tail DC motors shows their limitations in the admitted interval.

4.4. Test4: Experimental tracking in presence of wind effects

In order to show the robustness of the proposed control method, wind disturbances are added experimentally as presented in Fig. 25. The experimental results are depicted in Fig. 26(a and b), Fig. 29(a and b) and Fig. 32(a and b) which prove the absolute position of the TRMS in main and tail plan, when the wind gusts are introduced. The pursuit missions are successfully performed and the reference trajectories are followed with high precision. In addition, the proposed control method achieves a good rejecting the external disturbances which proves a good robustness. Fig. 27(a and b), Fig. 30(a and b) and Fig. 33(a and b) represents the tracking error and it's dynamics of main and tail subsystems, the dynamic response of neural network is showed in Fig. 28(a and b), Fig. 31(a and b) and Fig. 34(a and b).

It is also remarked that in Fig. 26(c and d), Fig. 29(c and d) and Fig. 32(c and d) the control input signals are bounded in the allowed interval.

4.5. Test5: Robustness test

To test the robustness of the TRMS with the proposed controller, another type of external disturbance is introduced by offering a small jerk to the main and tail rotors. According to the practical results of the TRMS depicted in Fig. 35(a and b), it can be observed that the TRMS with the proposed controller is robust to the external disturbances. Fig. 36(a and b) represents the tracking error and it's dynamics of main and tail subsystems, the dynamic response of neural network is showed in Fig. 37(a and b).

In Fig. 35(c and d), it is remarked a peaking phenomena happens in the input control signals to surmount the abrupt variations of TRMS

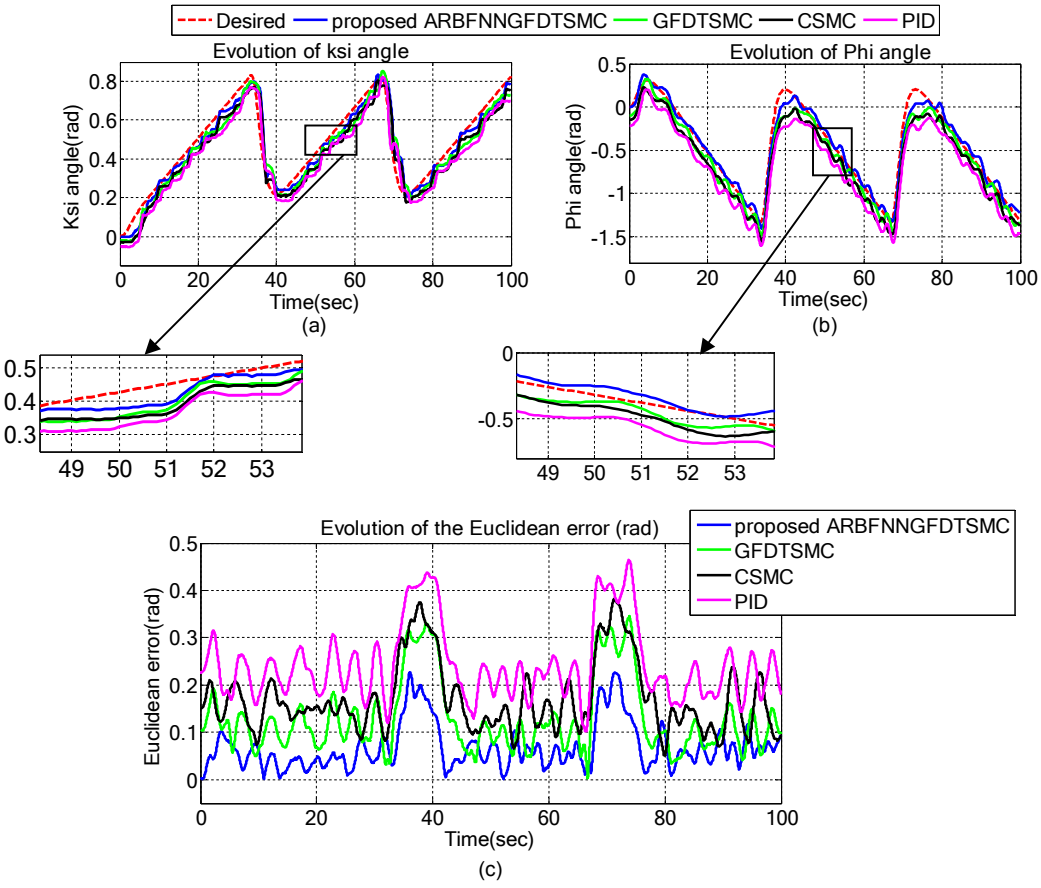

Fig. 39. Triangle wave tracking comparison between the proposed ARBFNNGFDTSMC, GFDTSMC, CSMC and PID control with wind effects.

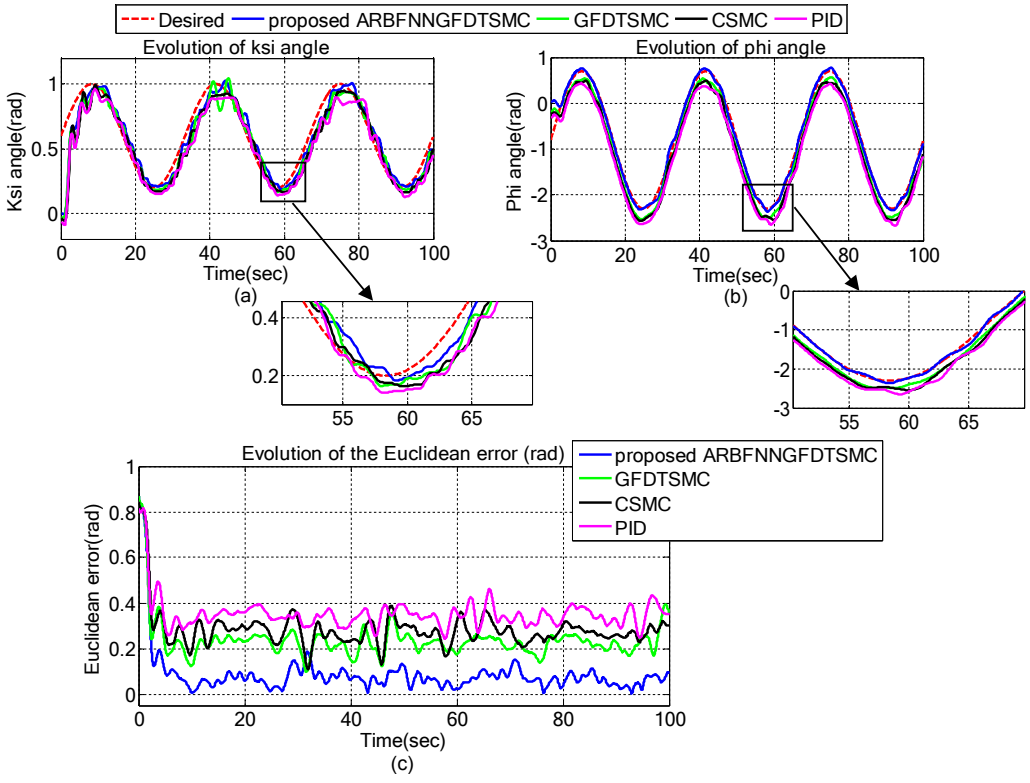

Fig. 40. Sine wave tracking comparison between the proposed ARBFNNGFDTSMC, GFDTSMC, CSMC and PID control with wind effects.

Table 2
RMSE values for the proposed ARBFNNGFDTSMC, GFDTSMC, CSMC and PID control.

Scenario	Controller Types	RMSE values (Rad)
Square wave tracking	Proposed ARBFNNGFDTSMC	**0.0982**
	GFDTSMC	0.1902
	CSMC	0.2331
	PID	0.3210
Triangle wave tracking	Proposed ARBFNNGFDTSMC	**0.1344**
	GFDTSMC	0.2017
	CSMC	0.2430
	PID	0.3278
Sine wave tracking	Proposed ARBFNNGFDTSMC	**0.2153**
	GFDTSMC	0.3452
	CSMC	0.3980
	PID	0.4755

angles, provoked by external disturbances. From experimental results, the proposed control method demonstrates a good performances of trajectory following.

In summary, from the tests presented in this section, it can be stated that the employs of the proposed ARBFNNGFDTSMC allows obtaining a high-performance control with a stabilize the TRMS in a reference position or follow a predefined trajectory. From implementation side, the time duration for the algorithm compilation is determined using one of the timers of the Advantech PCI 1711 card, which providing more bandwidth for data transmission and allowing faster read/write speed. The reported turnaround time (execution time) in the Simulink of the whole algorithm including the angles calculation $\psi$and φ angles (from the resolver), the reference angles, the voltages control inputs are transmitted to the TRMS and the proposed controller (solving differential equations using Simulink by Euler method) is inferior to sampling rate (real time). In addition the algorithm can be coded in C language, and based on the available powerful control cards (DSP, FPGA, dsPIC…), the processing time and CPU utilization will not be affected much by the execution of the proposed algorithm.

5. Performance comparison

To explore the effectiveness of the proposed ARBFNNGFDTSMC, a comparison between the tracking problem in presence of wind effects obtained using the proposed controller, the global fast dynamic terminal sliding mode control (GFDTSMC), the classical sliding mode control (CSMC) and the PID control, have been performed experimentally on the TRMS. The tracking responses of fours controllers are depicted in Fig. 38, Fig. 39 and Fig. 40. Therefore, as shown in Fig. 38(c), Fig. 39(c) and Fig. 40(c) the Euclidean error of the proposed controller is a significantly smaller than that of the conventional controllers due to the adaptive learning capabilities of ARBFNNGFDTSMC strategy.

For quantitative comparison between four previous control methods, root-mean-square error (RMSE) is used as the comparison criteria. Table.2 and Fig. 41 shows the RMSE values of the experimental results in presence of external disturbances (wind effects) using the GFDTSMC, CSMC and PID control and the ARBFNNGFDTSMC approach. It is observed that the proposed ARBFNNGFDTSMC offers the smallest values control of RMSE, whereas the PID control present the largest values of RMSE. It can be seen that the system performances are better, when using the proposed ARBFNNGFDTSMC as compared to the GFDTSMC, CSMC and PID control controllers.

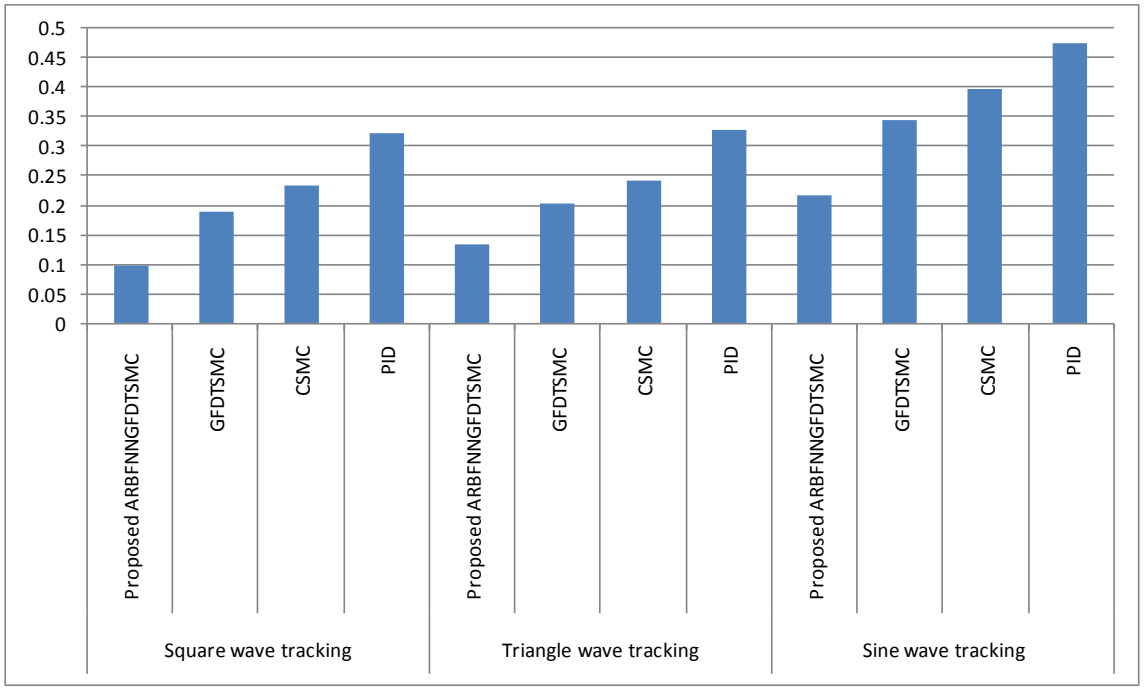

Fig. 41. RMSE Histogram of the proposed ARBFNNGFDTSMC, GFDTSMC, CSMC and PID control.

From the comparative study, it can been concluded that the proposed control strategy is characterized by robust trajectory tracking performance in presence of external disturbances such as wind effects, with - low tracking error and without exact knowledge of system parameters.

6. Conclusion

In this work, an experimental validation of ARBFNNGFDTSMC of TRMS which characterized by a high nonlinearities and cross-coupling effect between the main and tail subsystems. An adaptive RBFNN has been used in the proposed control design in order to identified unknown nonlinear dynamics of the TRMS. In addition, another adaptive control expressions has been added to diminish the wind gusts, external disturbance effects, and to compensate the estimation errors of the adaptive RBFNN.

In addition, by utilizing the Lyapunov method, it has been demonstrated that the closed-loop system with the developed controller is stable. The capability of the developed controller has been tested with several desired trajectories and it has been proven that the TRMS can follow reference trajectories with good precision. Also, it was proven in practical results that the developed controller has good robustness versus wind effects and better external disturbance rejection. Henceforth, with respect to the alluring capability of the proposed controller in real time, it might be utilized to control others types of non linear systems and unmanned aerial vehicles.

CRediT authorship contribution statement

Mohammed Zinelaabidine Ghellab: Methodology, Software. **Samir Zeghlache:** Supervision. **Ali Djerioui:** Visualization, Investigation. **Loutfi Benyettou:** Writing - review & editing.

Declaration of Competing Interest

The authors declare that they have no known competing financial interests or personal relationships that could have appeared to influence the work reported in this paper.

Appendix A. Supplementary material

Supplementary data to this article can be found online at https://doi.org/10.1016/j.measurement.2020.108472.

References

[1] K.V. Sudarshan, K. Rajul, K. Rahul, Design and real time implementation of *fmincon*, MOGA tuned IO-PID and FO-PI$^{\lambda}$D$^{\mu}$ controllers for stabilization of TRMS, Procedia Comput. Sci. 171 (2020) 1241–1250.

[2] K.P. Parthish, J. Jeevamma, H_2 Vs H_∞ control of TRMS via output error optimization augmenting sensor and control singularities, Ain Shams Eng. J. 11 (1) (2020) 77–85.

[3] T. Azamat, L.V. Andrea, M.M. Rafael, Complete dynamic model of the Twin Rotor MIMO System (TRMS) with experimental validation, Control Eng. Pract. 66 (2017) 89–98.

[4] N. Almtireen, H. Elmoaqet, M. Ryalat, Linearized modelling and control for a twin rotor system, Aut. Control Comp. Sci 52 (2018) 539–551.

[5] D.M. Ezekiel, R. Samikannu, M. Oduetse, Modelling of the twin rotor MIMO system (TRMS) using the first principles approach, in: Proceeding of IEEE International Conference on Computer Communication and Informatics (ICCCI), 2020, pp. 1–7.

[6] J. Wijekoon, Y. Liyanage, S. Welikala, L. Samaranayake, Yaw and pitch control of a twin rotor MIMO system, in: Proceeding of IEEE International Conference on Industrial and Information Systems (ICIIS), 2017, pp. 1–6.

[7] R.P. Borase, D.K. Maghade, S.Y. Sondkar, S.N. Pawar, A review of PID control, tuning methods and applications, Int. J. Dynam. Control (2020), https://doi.org/10.1007/s40435-020-00665-4.

[8] M.S. Meon, T.L. Mohamed, M.H. Ramli, M.Z. Mohamed, N.F. Manan, Review and Current Study on New Approach using PID Active Force Control (PIDAFC) of Twin Rotor Multi Input Multi Output System (TRMS), Humanities, Science and Engineering Research (SHUSER), Kuala Lumpur, Malaysia, 2012, pp. 163–167.

[9] R. Raul-Cristian, P. Radu-Emil, D. Radu-Codrut, Second order intelligent proportional-integral fuzzy control of twin rotor aerodynamic systems, Procedia Comput. Sci. 139 (2018) 372–380.

[10] P. Das, R.K. Mehta, O.P. Roy, Optimized methods for the pre-eminent performance of LQR control applied in a MIMO system, Int. J. Dynam. Control 7 (2019) 1501–1520.

[11] M. Ahmad, A. Ali, Choudhry MA fixed-structure H_∞ controller design for two-rotor aerodynamical system (TRAS), Arab. J. Sci. Eng. 41 (2016) 3619–3630.

[12] F. Faris, A. Moussaoui, B. Djamel, T. Mohammed, Design and real-time implementation of a decentralized sliding mode controller for twin rotor multi-input multi-output system. Proc. Inst. Mech. Eng. Part I: J. Syst. Control Eng. 231 (1) (2017) 3–13.

[13] C.W. Tao, J.S. Taur, Y.H. Chang, C.W. Chang, A novel fuzzy sliding and fuzzy integral sliding controller design for the twin rotor multi-input multi-output system, IEEE Trans. Fuzzy Syst. 18 (2010) 1–12.

[14] S. Mondal, C. Mahanta, Adaptive second-order sliding mode controller for a twin rotor multi-input multi-output system, IET Control Theory 6 (14) (2012) 2157–2167.

[15] C. Mishra, S.K. Swain, M.S. Kumar, S.K. Yadav, Fractional order sliding mode controller for the twin rotor MIMO system, in: Proceeding of IEEE International Conference on Intelligent Computing and Control Systems (ICCS), Madurai, India, 2019, pp. 662–667.

[16] R. Chithra, T. Koshy, Robust optimal sliding mode control of twin rotor MIMO system, Int. J. Eng. Res. Technol. 5 (9) (2016) 111–115.

[17] N. Bouarroudj, A. Djari, D. Boukhetala, F. Boudjema, Tuning of decentralized fuzzy logic sliding mode controller using PSO algorithm for nonlinear Twin Rotor Mimo System, in: Proceeding of IEEE International Conference on Systems and Control (ICSC), 2017, pp. 45–50.

[18] K. Dheeraj, J. Jacob, M.P. Nandakumar, Direct adaptive neural control design for a class of nonlinear multi input multi output systems, IEEE Access 7 (2019) 15424–15435.

[19] A. Rahideh, A.H. Bajodah, M.H. Shaheed, Real time adaptive nonlinear model inversion control of a twin rotor MIMO system using neural networks, Eng. Appl. Artif. Intell. 25 (6) (2012) 1289–1297.

[20] A. Chelihi, M. Chemachema, Model reference adaptive control for twin rotor multiple-input and multiple-output system via minimal controller synthesis, Proc. Inst. Mech. Eng. I: J. Syst. Control Eng. 228 (6) (2014) 406–418.

[21] B. Pratap, S. Purwar, Real-time implementation of neuro adaptive observer-based robust backstepping controller for twin rotor control system, J. Control. Autom. Electr. Syst. 25 (2) (2014) 137–150.

[22] M. Chemachema, S. Zeghlache, Output feedback linearization based controller for a helicopter-like twin rotor MIMO system", J. Intell. Robot Syst. 48 (1) (2014) 181–190.

[23] J.G. Juang, M.T. Huang, W.K. Liu, PID control using presearched genetic algorithms for a MIMO system, IEEE Trans. Syst. Man Cybern.: Part C. 38 (2008) 716–727.

[24] J.G. Juang, W.K. Liu, R.W. Lin, A hybrid intelligent controller for a twin rotor MIMO system and its hardware implementation, ISA Trans. 50 (2011) 609–619.

[25] R. Raghavan, S. Thomas, Practically implementable model predictive controller for a twin rotor multi-input multi-output system, J. Control Autom. Electr. Syst. 28 (2017) 358–370.

[26] N.V. Chi, Adaptive feedback linearization control for twin rotor multiple-input multiple-output system, Int. J. Control Autom. Syst. 15 (2017) 1267–1274.

[27] Twin Rotor MIMO System Manual, Feedback Instruments Ltd., UK, 2006.

[28] L. Moussa, C. Mohamed, Robust adaptive nonsingular fast terminal sliding-mode tracking control for an uncertain quadrotor UAV subjected to disturbances, ISA Trans. 99 (2020) 290–304.

[29] H.H. Joel, S.C. Sergio, L. Ricardo, G.M. Arturo, L. Rogelio, Robust nonsingular fast terminal sliding-mode control for Sit-to-Stand task using a mobile lower limb exoskeleton, Control Eng. Pract. 101 (2020) 104496.

[30] X. Jing-Jing, Z. Guo-Bao, Global fast dynamic terminal sliding mode control for a quadrotor UAV, ISA Trans. 66 (2017) 233–240.

[31] Y. Fouad, B. Omar, H. Mustapha, R. Nassim, Observer-based adaptive fuzzy backstepping tracking control of quadrotor unmanned aerial vehicle powered by Li-ion battery, J. Intell. Robot Syst. 84 (2016) 179–197.

[32] N. Bounar, A. Boulkroune, F. Boudjema, M. M'Saad, M. Farza, Adaptive fuzzy vector control for a doubly-fed induction motor, Neurocomputing (2015).